



Hafnium isotopic disequilibrium during sediment melting and assimilation

C. Zhang, D. Liu, X. Zhang, C. Spencer, M. Tang, J. Zeng, S. Jiang, Marc Jolivet, X. Kong

► To cite this version:

C. Zhang, D. Liu, X. Zhang, C. Spencer, M. Tang, et al.. Hafnium isotopic disequilibrium during sediment melting and assimilation. *Geochemical Perspectives Letters*, 2020, 12, pp.34-39. 10.7185/geochemlet.2001 . insu-02453795

HAL Id: insu-02453795

<https://insu.hal.science/insu-02453795>

Submitted on 24 Jan 2020

HAL is a multi-disciplinary open access archive for the deposit and dissemination of scientific research documents, whether they are published or not. The documents may come from teaching and research institutions in France or abroad, or from public or private research centers.

L'archive ouverte pluridisciplinaire **HAL**, est destinée au dépôt et à la diffusion de documents scientifiques de niveau recherche, publiés ou non, émanant des établissements d'enseignement et de recherche français ou étrangers, des laboratoires publics ou privés.

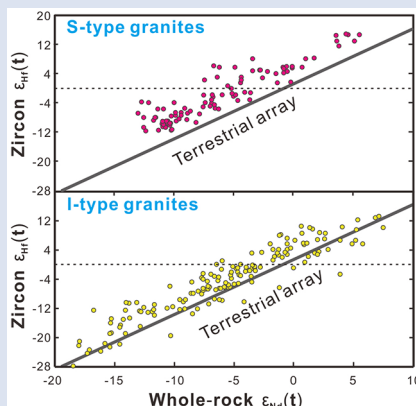
Hafnium isotopic disequilibrium during sediment melting and assimilation

C. Zhang^{1,2}, D. Liu^{1,3*}, X. Zhang⁴, C. Spencer^{5,6},
M. Tang⁷, J. Zeng^{1,2}, S. Jiang⁸, M. Jolivet⁹, X. Kong^{1,2}

OPEN  ACCESS

doi: 10.7185/geochemlet.2001

Abstract



Identification of juvenile and mature crustal sources in granite formation relies on radiogenic isotopic systems such as Sm-Nd and Lu-Hf and assumes isotope systems reach equilibrium between the melt and residual phases prior to melt extraction. However, we hypothesise disequilibrium melting and residual zircon result in preferential retention of ^{177}Hf in residues, generating partial melts with higher $^{176}\text{Hf}/^{177}\text{Hf}$ ratios. To test this hypothesis, we evaluate radiogenic isotopic signatures of strongly-peraluminous granites from the Chinese Altai. These granites show Nd-Hf isotopic decoupling and inherited zircons with negative $\epsilon_{\text{Hf}}(t)$ values providing evidence for incomplete Hf release. This is consistent with the significant depletions in Zr and Hf. The Chinese data compilation shows that strongly-peraluminous and calcic to calc-alkalic, magnesian metaluminous or ferroan peraluminous (often respectively referred to as S- and I-type) granites show elevated $\epsilon_{\text{Hf}}(t)$ relative to the terrestrial Hf-Nd isotopic array. Hf isotope disequilibrium marked by the preferential release of radiogenic Hf is likely ubiquitous during anatexis of zircon-rich protoliths.

Received 1 June 2019 | Accepted 24 November 2019 | Published 15 January 2020

Introduction

Strongly-peraluminous granites (SPG) generally indicate that partial melting of metasedimentary crustal rocks has been occurring throughout Earth's history (Harris *et al.*, 2000; Appleby *et al.*, 2010; Bucholz and Spencer, 2019). Experimental and geodynamic modelling have been applied to understanding the chemistry and physics of partial melting processes (Sawyer *et al.*, 1991, 2011). It is assumed that crustal partial melts inherit the radiogenic isotope composition of their protoliths. Hafnium (Hf) is a geochemically important element in zircon because its isotopic composition is a sensitive tracer of crustal and mantle processes (Kemp *et al.*, 2006). Zircon retains the initial melt isotopic composition because of its low Lu/Hf ratio and refractory nature in sedimentary processes (Andersen *et al.*, 2002). However, studies of SPG have shown the Hf isotopic composition of partial melts may not match the inferred magma source (Belousova *et al.*, 2005; Villarros *et al.*, 2012; Iles *et al.*, 2019). Residual zircons,

i.e. not dissolved during partial melting, may retain a significant amount of unradiogenic Hf (i.e. low $^{176}\text{Hf}/^{177}\text{Hf}$) causing the derivative crustal melts to have higher $^{176}\text{Hf}/^{177}\text{Hf}$ ratios relative to the bulk source (Farina *et al.*, 2014). In such cases, source composition and melting conditions exert a first order control on Hf isotopic equilibrium during anatexis (Tang *et al.*, 2014). To test the residual zircon effect on Hf isotopes in granitic rocks, we carried out a Nd-Hf-O isotopic study of SPG in the Chinese Altai. We then evaluate the generality of residual zircon effect in granitic magmatism using a compiled Nd-Hf isotope database.

The Central Asian Orogenic Belt (CAOB) is Earth's largest Phanerozoic accretionary orogen (Kröner *et al.*, 2014). The Chinese Altai is located in the central CAOB (Fig. S-1a), with >40 % of the exposed rocks being granites (Zhang *et al.*, 2017). Previous studies dated CAOB plutons as Late Ordovician-Devonian (450 to 370 Ma) and Permian (280 to 270 Ma) and also report Nd-Hf isotopic decoupling in these granites (e.g., Zhang *et al.*, 2017). This paper reports new U-Pb

1. State Key Laboratory of Petroleum Resources and Prospecting, China University of Petroleum, Beijing, China
 2. College of Geoscience, China University of Petroleum, Beijing, China
 3. Unconventional Petroleum Research Institute, China University of Petroleum, Beijing, China
 4. School of Earth Sciences and Gansu Key Laboratory of Mineral Resources in Western China, Lanzhou University, Lanzhou 730000, China
 5. TIGeR (The Institute of Geoscience Research), School of Earth and Planetary Science, Curtin University, Perth, Australia
 6. Department of Geological Sciences and Geological Engineering, Queen's University, Kingston, ON, Canada
 7. Department of Earth, Environmental and Planetary Sciences, Rice University, Houston, TX, USA
 8. Energy and Geoscience Institute, University of Utah, Salt Lake City, UT, USA
 9. Géosciences Rennes, CNRS — Université Rennes 1, Rennes, France
- * Corresponding author (email: liudd@cup.edu.cn)



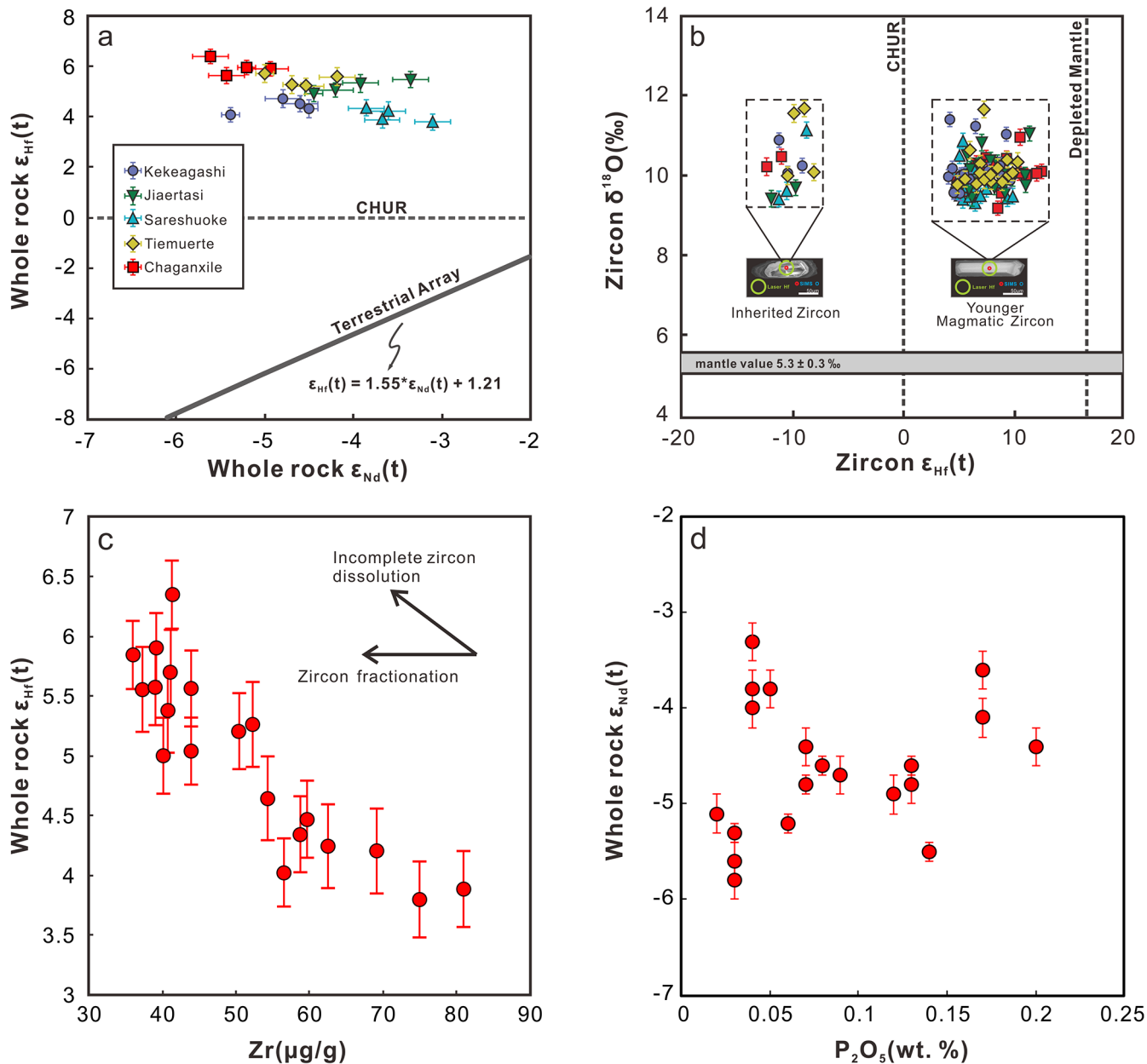


Figure 1 (a) $\epsilon_{\text{Hf}}(t)$ versus $\epsilon_{\text{Nd}}(t)$ for SPG in the Chinese Altai calculated based on U-Pb ages of the various plutons. Terrestrial array equations are from Vervoort et al. (2011). (b) Zircon $\epsilon_{\text{Hf}}(t)$ versus zircon $\delta^{18}\text{O}$ for SPG in the Chinese Altai. Mantle values after Valley et al. (1998). Inherited zircons show $\epsilon_{\text{Hf}}(t)$ and $\delta^{18}\text{O}$ values, indicating a metasedimentary source. Younger magmatic zircons show positive $\epsilon_{\text{Hf}}(t)$ values and similarly high $\delta^{18}\text{O}$ values, CHUR-chondritic uniform reservoir. (c) $\epsilon_{\text{Hf}}(t)$ versus Zr ($\mu\text{g/g}$). (d) $\epsilon_{\text{Nd}}(t)$ versus P_2O_5 (wt. %). Uncertainties of all isotope measurements are internal 2σ .

ages, Nd-Hf-O isotopic compositions, major and trace element geochemistry, and Hf-O isotopes of inherited zircons within SPG samples from the Chinese Altai with the aim of providing insights into SPG melting processes and isotope systematics.

Methods and Results

Granite samples from the Kekeagashi, Tiemuerte, Jiaertasi, Chaganxile, and Sareshuoke plutons in the Chinese Altai (Fig. S-2b) were analysed. *In situ* zircon U-Pb analysis was performed using laser ablation inductively coupled plasma mass spectrometry (ICP-MS). Whole rock (WR) major/trace element compositions were analysed using X-ray fluorescence spectrometry and inductively coupled plasma mass spectrometry. Nd isotope measurements were conducted using a MAT-262 thermal ionisation mass spectrometer in static mode.

Hf isotope measurements were analysed using Nu Plasma II ICP-MS. *In situ* zircon Hf isotope analyses were conducted using a Thermo Scientific Neptune ICP-MS coupled to a 193-nm laser. *In situ* zircon O isotope analyses were conducted using a Cameca IMS-1280HR secondary ion mass spectrometer. Details of analytical methods are provided in Supplementary Information.

Zircon U-Pb ages show granite crystallisation between 437 and 409 Ma (Fig. S-2). U-Pb dating of inherited zircon cores indicate that Palaeozoic zircon grains seeded on significantly older crystals, with ages ranging from 3506 to 1990 Ma (Fig. S-3). The WR $\epsilon_{\text{Nd}}(t)$ and $\epsilon_{\text{Hf}}(t)$ values range from -5.6 to -3.1 and +3.8 to +6.3, respectively. The $\delta^{18}\text{O}$ and $\epsilon_{\text{Hf}}(t)$ values of the magmatic zircon rims spanned from +9.2 to +11.6 ‰ and +4.0 to +12.3, respectively. The $\delta^{18}\text{O}$ values of zircon cores range from +9.3 to +11.8 ‰ and $\epsilon_{\text{Hf}}(t)$ values from -12.4 to -8.2. Data are available in Tables S-1 and S-2.

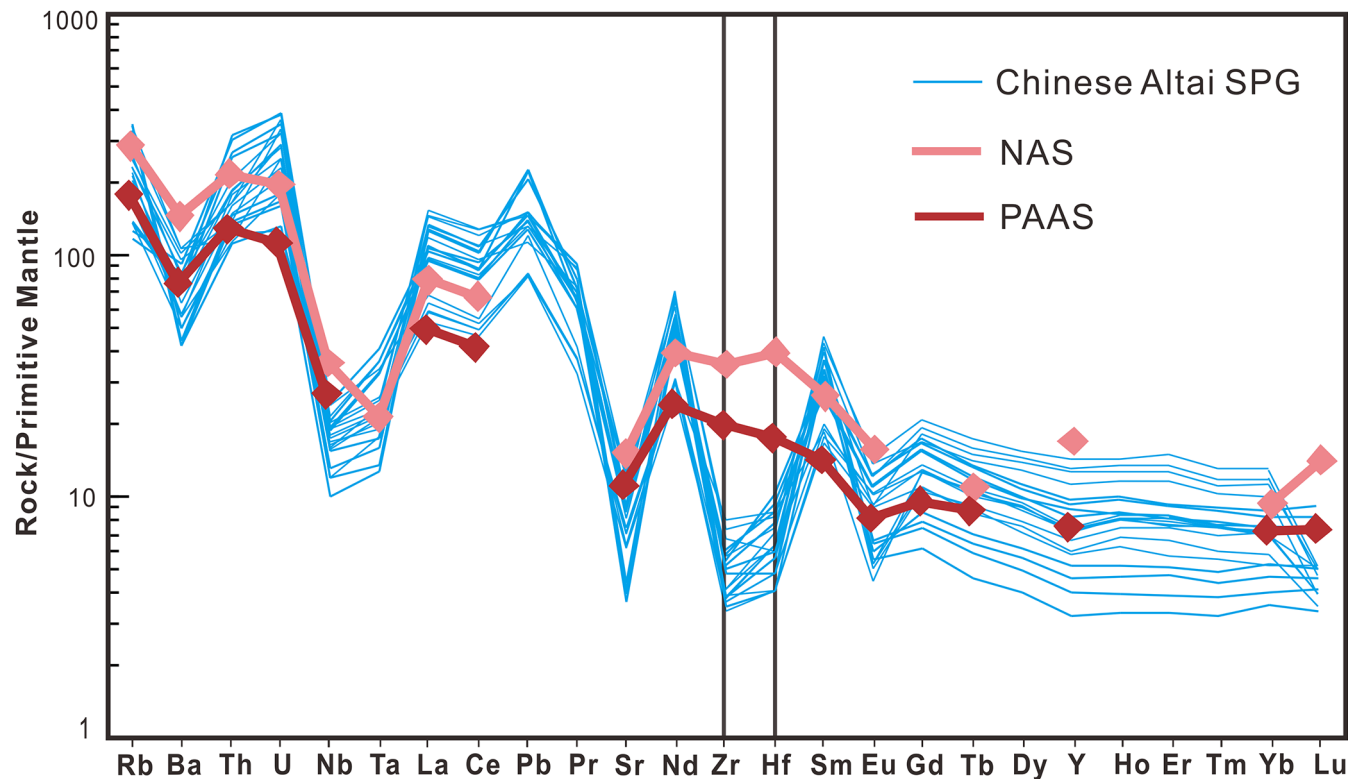


Figure 2 Primitive mantle-normalised trace element spider patterns of the studied granites, PAAS and NAS. Normalisation data from Sun and McDonough (1989). Note the Zr-Hf depletions of the SPG from this study. All the data are listed in Table S-4.

Discussion and Implications

High $\delta^{18}\text{O}$ values (+9.2 to +11.6 ‰), low $\epsilon_{\text{Nd}}(t)$ values (−5.6 to −3.1), strongly-peraluminous character ($A/\text{CNK} = 1.1\text{-}1.3$), presence of aluminous minerals (*i.e.* garnet, sillimanite, cordierite, and muscovite; Fig. S-4), and low Fe, Mg, Ca, and Na contents are consistent with derivation of melted sediment (Chappell and White, 1974).

The highly radiogenic Hf isotopes of these SPG and Nd-Hf isotopic decoupling (Fig. 1a) give contradictory implications as to the contributions of isotopically depleted and enriched materials. It is feasible that Nd-Hf isotopic decoupling is either highlighting differential source signature or caused by crustal melting processes. Mineral sorting effects during sediment transport can concentrate zircon in coarse-grained sedimentary rocks while fine-grained, clay-rich rocks are nearly devoid of zircon (Carpentier *et al.*, 2009). Consequently, zircon-depleted sediments tend towards radiogenic Hf isotope signatures, while zircon-rich sediments generally have unradiogenic Hf isotope compositions. Melting of fine-grained, zircon-poor sedimentary rocks is likely to produce magmas with radiogenic Hf isotope compositions relative to their Nd isotope composition and account for a negative correlation between magma $\epsilon_{\text{Hf}}(t)$ and Zr concentration (Fig. 1c). However, we suggest that this mechanism is unlikely to be responsible for isotopic decoupling in the investigated granites as; 1) the sedimentary rocks in the studied area are sandstones and mudstones that are enriched in zircon and have moderate to low Nd/Hf ratios (from 0.8 to 3.8, Long *et al.*, 2008); 2) fine-grained clastic sedimentary proxies (Post-Archean Australian Shales [PAAS] and North American Shales [NAS]), are not depleted in Zr and Hf while SPG of the Chinese Altai are depleted in Zr and Hf (Fig. 2); 3) inherited zircon cores are abundant in SPG, suggesting the source is not zircon-depleted. Thereby, we therefore conclude that radiogenic Hf isotopes are not source signatures nor is Nd-Hf isotopic decoupling due to melting of zircon-poor fine-grained sediments.

Nd-Hf isotopic decoupling may also be generated by disequilibrium melting with incomplete zircon dissolution (Fig. S-5; Zeng *et al.*, 2005; Farina *et al.*, 2014; Tang *et al.*, 2014; Iles *et al.*, 2018). Because Hf diffusion in zircon is slow under crustal melting conditions (Watson and Harrison, 1983), Hf isotope equilibrium during crustal anatexis is largely controlled by zircon dissolution. Inherited zircons in our samples are evidence of incomplete zircon dissolution during anatexis. Residual zircon in magma sources can retain unradiogenic Hf (*i.e.* low $^{176}\text{Hf}/^{177}\text{Hf}$) and may produce partial melts with elevated $\epsilon_{\text{Hf}}(t)$ relative to the source. This model explains Hf isotope variability recorded by zircon crystallising during partial melting and inherited zircon dissolution. This may generate melt batches with variable Hf isotope compositions, even if melts come from a single source (Tang *et al.*, 2014). This single source melting scenario is supported by the zircon O isotopic compositions for the Chinese Altai granites. If the variation in zircon Hf isotopic composition is due to mixing between mantle-derived magmas and metasedimentary materials, negative correlations between zircon $\epsilon_{\text{Hf}}(t)$ and zircon $\delta^{18}\text{O}$ (Kemp *et al.*, 2007) are expected. However, Chinese Altai granites show similar $\delta^{18}\text{O}$ (cores: +9.3 to +11.8 ‰; rims: +9.2 to +11.6 ‰) despite the large Hf isotopic variation (>20 epsilon units; Fig. 1b).

Disequilibrium melting with residual zircon can explain strong Zr and Hf depletions in the Chinese Altai granites (Fig. 2) as zircon hosts most Zr and Hf. More importantly, the WR and zircon $\epsilon_{\text{Hf}}(t)$ values of SPG correlate negatively with Zr concentrations (Fig. 1c), which is expected if residual zircon controls Hf isotopes and Zr and Hf concentrations in partial melts. Zircon fractionation during magma differentiation may also cause Zr and Hf depletions, but would not produce negative correlations between Hf isotopic composition and Zr concentration.

Nd concentrations in the melt and residue are dominantly controlled by apatite and monazite (Zeng *et al.*, 2005). Nd isotopes may be affected by disequilibrium melting with



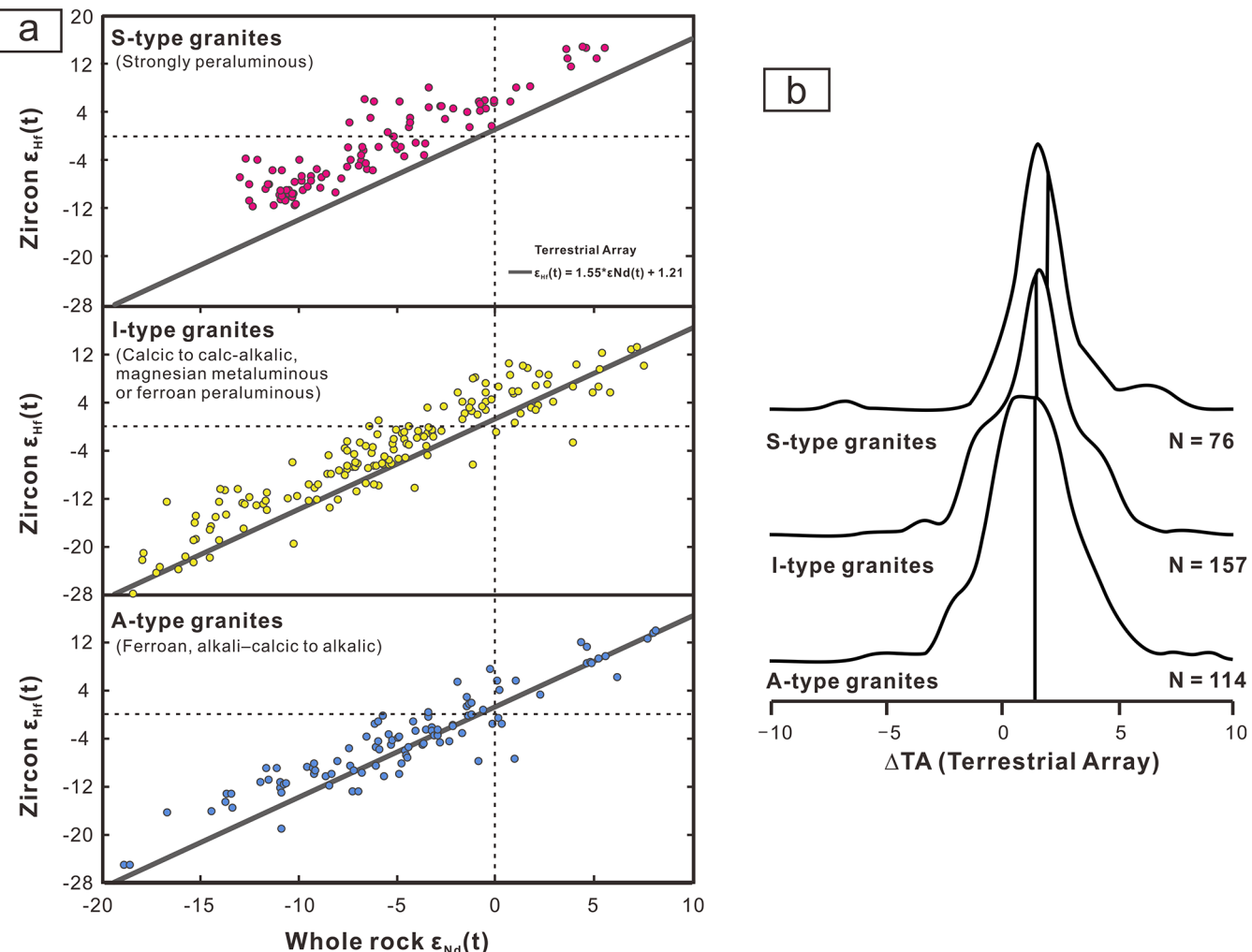


Figure 3 (a) Compilation of published neodymium and hafnium isotopic compositions of I-type, A-type, and S-type granites (as defined in the figure). Points represent average zircon values from single plutons. References listed in Table S-3. (b) Distance from the terrestrial array (TA) expressed as ΔTA calculated for the three granite groups. Vertical line represents the median of all of the samples and demonstrate an increasing shift towards greater Hf disequilibrium (above the TA) with increasing aluminosity.

residual apatite and monazite. However, zircon has extremely low Lu/Hf and thus strongly fractionates Hf from Lu while apatite and monazite only moderately fractionate Nd and Sm. Therefore, Hf isotopes are more sensitive to disequilibrium melting than Nd isotopes even if both zircon and P-bearing accessory minerals are present in the residues. This is supported by the observation that $\epsilon_{\text{Hf}}(t)$ strongly correlates with Zr concentration while $\epsilon_{\text{Nd}}(t)$ varies independently from P₂O₅ in our samples (Fig. 1d). We suggest that Nd-Hf decoupling of Altai SPG is caused by the Hf isotopic disequilibrium and incomplete zircon dissolution during sediment melting. Mineral sorting might have a minor contribution to isotopic decoupling in zircon-rich sources.

To evaluate the generality of residual zircon effects in granitic magmatism, we compiled a database of Chinese granite Nd-Hf isotope compositions. Nd-Hf isotopic decoupling is present in SPG with systematically elevated $\epsilon_{\text{Hf}}(t)$ relative to the terrestrial Nd-Hf isotope array (TA) and is also present to a lesser degree in I-type (calcic to calc-alkalic, magnesian metaluminous or ferroan peraluminous) granites (Fig. 3). This is in contrast to A-type (ferroan, alkali-calcic to alkalic) granites that overlap with the TA. We calculated minimum temperatures required to dissolve zircon completely in the source rocks (Fig. 4). We assume the melting degree to be ~30 % (Petford *et al.*, 2000). Our calculation shows that,

for peraluminous melts ($M > 1.1$), complete zircon dissolution would require >950 °C if the source contains >200 µg/g Zr, which appears to be too high for most SPG systems. Considering that the average PAAS and NAS contains 210 and 200 µg/g Zr, respectively (Gromet *et al.*, 1984; Taylor and McLennan, 1985), residual zircon seems to be inevitable if the source rocks are detritus-rich sedimentary rocks. I-type granites also deviate from the TA to a lesser degree than SPG but greater than A-type granite implying sediment assimilation in typical arc settings (Fig. 3). We suggest that may also be explained by a residual zircon effect if zircon is present in the sources of I-type granites.

These findings raise questions to the utility of Hf isotopes in quantifying crustal recycling as disequilibrium melting and residual zircon may lead to radiogenic Hf isotopes in the partial melts that falsely indicate juvenile sources. Therefore, Hf isotopes of SPG and I-type granites may not faithfully reflect the protoliths. Hf isotopes biased by residual zircon may lead to erroneous conclusions in detrital zircon studies as petrogenetic context is missing. Rates of crustal reworking can be significantly underestimated if only Hf isotopes are applied. Therefore, caution is needed when using detrital zircon Hf isotopes to reconstruct the net growth of the continental crust.

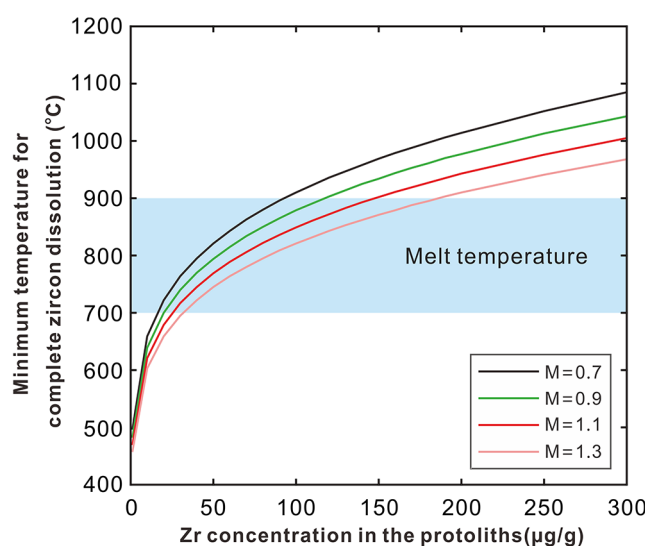


Figure 4 Calculated minimum melt temperature for zircon dissolution as a function of Zr concentration in the protoliths and M value (cation ratio). SPG have M values > 1.1 while I-type granites typically have M values < 1.0. Melt Zr concentration at zircon saturation using the zircon saturation model of Boehnke et al. (2013).

Acknowledgements

The manuscript was greatly improved by constructive reviews from Claire Bucholz, Kieran Iles and an anonymous reviewer and the editor, Horst R. Marschall. We thank William L. Griffin, Keda Cai for the valuable discussions. This work is financially supported by the grants from the National Natural Science Foundation of China (No. 41502209), and the National Science and Technology Major Project (No. 2016ZX05034-001, 2017ZX05035-002).

Editor: Horst R. Marschall

Additional Information

Supplementary Information accompanies this letter at <http://www.geochemicalperspectivesletters.org/article2001>.



This work is distributed under the Creative Commons Attribution Non-Commercial No-Derivatives 4.0 License, which permits unrestricted distribution provided the original author and source are credited. The material may not be adapted (remixed, transformed or built upon) or used for commercial purposes without written permission from the author. Additional information is available at <http://www.geochemicalperspectivesletters.org/> copyright-and-permissions.

Cite this letter as: Zhang, C., Liu, D., Zhang, X., Spencer, C., Tang, M., Zeng, J., Jiang, S., Jolivet, M., Kong, X. (2020) Hafnium isotopic disequilibrium during sediment melting and assimilation. *Geochem. Persp. Let.* 12, 34–39.

References

- ANDERSEN, T. (2002) Correction of common lead in U-Pb analyses that do not report ^{204}Pb . *Chemical Geology* 192, 59–79.
- APPLEBY, S.K., GILLESPIE, M.R., GRAHAM, C.M., HINTON, R.W., OLIVER, G.J.H., KELLY, N.M. (2010) Do S-type granites commonly sample infracrustal sources? New results from an integrated O, U-Pb and Hf isotope study of zircon. *Contributions to Mineralogy and Petrology* 160, 115–132.
- BELOUSOVA, E.A., GRIFFIN, W.L., O'REILLY, S.Y. (2005) Zircon crystal morphology, trace element signatures and Hf isotope composition as a tool for petrogenetic modelling: examples from Eastern Australian granitoids. *Journal of Petrology* 47, 329–353.
- BOEHNKE, P., WATSON, E.B., TRAIL, D., HARRISON, T.M., SCHMITT, A.K. (2013) Zircon saturation re-revisited. *Chemical Geology* 351, 324–334.
- BUCHOLZ, C.E., SPENCER, C.J. (2019) Strongly peraluminous granites across the Archean-Proterozoic transition. *Journal of Petrology* 60, 1299–1348.
- CARPENTIER, M., CHAUVEL, C., MAURY, R.C., MATTIELLI, N. (2009) The “zircon effect” as recorded by the chemical and Hf isotopic compositions of Lesser Antilles forearc sediments. *Earth and Planetary Science Letters* 287, 86–99.
- CHAPPELL, B., WHITE, A. (1974) Two contrasting granite types. *Pacific Geology* 8, 173–174.
- FARINA, F., STEVENS, G., GERDES, A., FREI, D. (2014) Small-scale Hf isotopic variability in the Peninsula pluton (South Africa): the processes that control inheritance of source $^{176}\text{Hf}/^{177}\text{Hf}$ diversity in S-type granites. *Contributions to Mineralogy and Petrology* 168, 1065.
- GROMET, L.P., HASKIN, L.A., KOROTEV, R.L., DYMEK, R.F. (1984) The “North American shale composite”: Its compilation, major and trace element characteristics. *Geochimica et Cosmochimica Acta* 48, 2469–2482.
- HARRIS, N., VANCE, D., AYRES, M. (2000) From sediment to granite: timescales of anatexis in the upper crust. *Chemical Geology* 162, 155–167.
- ILES, K.A., HERGT, J.M., WOODHEAD, J.D. (2018) Modelling isotopic responses to disequilibrium melting in granitic systems. *Journal of Petrology* 59, 87–113.
- ILES, K.A., HERGT, J.M., WOODHEAD, J.D. (2019) Petrogenesis of granitoids from the Lachlan Fold Belt, southeastern Australia: the role of disequilibrium melting. *Gondwana Research* <https://doi.org/10.1016/j.gr.2019.08.011>.
- KEMP, A.I.S., HAWKESWORTH, C.J., PATERSON, B.A., KINNY, P.D. (2006) Episodic growth of the Gondwana supercontinent from hafnium and oxygen isotopes in zircon. *Nature* 439, 580.
- KEMP, A.I.S., HAWKESWORTH, C.J., FOSTER, G.L., PATERSON, B.A., WOODHEAD, J.D., HERGT, J.M., GARY, C.M., WHITEHOUSE, M.J. (2007) Magmatic and crustal differentiation history of granitic rocks from Hf-O isotopes in zircon. *Science* 315, 980–983.
- KRÖNER, A., KOVACH, V., BELOUSOVA, E., HEGNER, E., ARMSTRONG, R., DOLGOPOLOVA, A., SELTMANN, R., ALEXEIEV, D.V., HOFFMANN, J.E., WONG, J., SUN, M., CAI, K., WANG, T., TONG, Y., WILDE, S.A., DEGTYAREV, K.E., RYTSK, E. (2014) Reassessment of continental growth during the accretionary history of the Central Asian Orogenic Belt. *Gondwana Research* 25, 103–125.
- LONG, X.P., SUN, M., YUAN, C., XIAO, W.J., CAI, K.D. (2008) Early Paleozoic sedimentary record of the Chinese Altai. implications for its tectonic evolution. *Sedimentary Geology* 208, 88–100.
- PETFORD, N., CRUDEN, A.R., MCCAFFREY, K.J., VIGNERESSE, J.L. (2000) Granite magma formation, transport and emplacement in the Earth's crust. *Nature* 408, 669–673.
- SAWYER, E.W. (1991) Disequilibrium melting and the rate of melt-residuum separation during migmatization of mafic rocks from the Grenville Front, Quebec. *Journal of Petrology* 32, 701–738.
- SAWYER, E.W., CESARE, B., BROWN, M. (2011) When the Continental Crust Melts. *Elements* 7, 229–234.
- SUN, S.S., McDONOUGH, W.F. (1989) Chemical and isotopic systematics of oceanic basalts: implications for mantle composition and processes. *Geological Society, London, Special Publications* 42, 313–345.
- TANG, M., WANG, X.L., SHU, X.J., WANG, D., YANG, T., GOPON, P. (2014) Hafnium isotopic heterogeneity in zircons from granitic rocks: Geochemical evaluation and modeling of “zircon effect” in crustal anatexis. *Earth and Planetary Science Letters* 389, 188–199.
- TAYLOR, S.R., MCLENNAN, S.M. (1986) The chemical composition of the Archean crust. *Geological Society, London, Special Publications* 24, 173–178.
- VALLEY, J.W., KINNY, P.D., SCHULZE, D.J., SPICUZZA, M.J. (1998) Zircon megacrysts from kimberlite: oxygen isotope variability among mantle melts. *Contributions to Mineralogy and Petrology* 133, 1–11.
- VERVOORT, J.D., PLANK, T., PRYTULAK, J. (2011) The Hf-Nd isotopic composition of marine sediments. *Geochimica et Cosmochimica Acta* 75, 5903–5926.

- VILLAROS, A., BUICK, I.S., STEVENS, G. (2012) Isotopic variations in S-type granites: an inheritance from a heterogeneous source? *Contributions to Mineralogy and Petrology* 163, 243–257.
- WATSON, E.B., HARRISON, T.M. (1983) Zircon saturation revisited: temperature and composition effects in a variety of crustal magma types. *Earth and Planetary Science Letters* 64, 295–304.
- ZENG, L., ASIMOW P.D., SALEEBY J.B. (2005) Coupling of anatetic reactions and dissolution of accessory phases and the Sr and Nd isotope systematics of anatetic melts from a metasedimentary source. *Geochimica et Cosmochimica Acta* 69, 3671–3682.
- ZHANG, C., LIU, L.F., SANTOSH, M., LUO, Q., ZHANG, X. (2017) Sediment recycling and crustal growth in the Central Asian Orogenic Belt: Evidence from Sr-Nd-Hf isotopes and trace elements in granitoids of the Chinese Altay. *Gondwana Research* 47, 131–141.



Hafnium isotopic disequilibrium during sediment melting and assimilation

C. Zhang, D. Liu *, X. Zhang, C. Spencer, M. Tang, J. Zeng, S. Jiang, M. Jolivet, X. Kong

Supplementary Information

The Supplementary Information includes:

- Analytical methods
- Tables S-1 to S-5
- Figures S-1 and S-6
- Supplementary Information References

Analytical methods

Zircon U-Pb dating

Analytical methods for determination of zircon U-Pb ages are described in Zhang *et al.* (2019). The data for reference materials are listed in Table S-5-1.

Major and trace element analysis

Analytical methods for determination of whole-rock major and trace element are reported in Zhang *et al.* (2019). The data for reference materials are listed in Table S-5-2.

Whole rock Nd isotopic analysis

Four samples were collected for each pluton, and they were ground into powders, followed by introduction of isotope tracers and dissolution by HF + HNO₃ acid in Teflon capsules. Separation of Nd was conducted on HDEHP columns where there was a 0.18 N HCl elutant. Nd isotopic analysis was accomplished at the Tianjin Institute of Geology and Mineral Resources using a thermal ionization mass spectrometry (TIMS). As identified in this research, La Jolla and BCR-1 standards were applied to control analytical quality. Detailed procedures for preparation of samples and subsequent analyses conform to those in Li *et al.* (2015). The data for reference materials are listed in Table S-5-3.

Whole rock Hf isotopic analysis

Granitic rock powders were mixed with 0.5 ml of 60 wt. % HNO₃ and 1.0 ml of 40 wt. % HF in high-pressure PTFE bombs, followed by steel-jacketing and were then placed in the oven at 195 °C for 3 days to ensure absolute digestion. Subsequently, the digestion solution was dried on an electric hot plate, and got reconstituted into 1.5 ml of 1.5 mol/L HCl. A Biorad AG50W-X8 cation exchange column was used to wash out high field strength elements using the 1.5 mol/L HCl, and these samples were then dried and re-dissolved in 3.0 mol/L HCl. The obtained solution was dropped into the LN exchange column, followed by elution of



Titanium using a 4.0 mol/L HCl + 0.5 wt. % H₂O₂ mixture. Finally, the Hf component was extracted from the column with 2.0 mol/L HF. After undergoing a slow drying process, the Hf component was re-dissolved in 1.0 ml of 2 wt. % HNO₃, which was prepared as the mother solution. 100 μ l of the mother solution was then diluted to 1.0 ml of solution for precise elemental content measurement on an Agilent Technologies 7700x quadrupole ICP-MS device. Subsequently, at the State Key Laboratory of Continental Dynamics, Northwest University, Xi'an, an Aridus II desolvating nebulizer system manufactured by the Teledyne Cetac Technologies Company was used to dilute the solution (40 ppb Hf) into the Nu Instruments Nu Plasma II MC-ICP-MS. Normalisation to $^{179}\text{Hf}/^{177}\text{Hf} = 0.7325$ was implemented to internally correct the raw isotopic ratio data for mass fractionation. Periodic analysis of international isotopic standards (Alfa Hf) was carried out to take possible instrumental drift into consideration. Quality control was ensured by referring to USGS, RGM-2, AVG-2, BHVO-2, and BCR-2 materials. These isotopic results agreed with previous publications within analytical uncertainty (Weis *et al.*, 2007). The data for reference materials are listed in Table S-5-4.

In situ zircon Hf isotopic measurement

We implemented *in-situ* zircon Hf isotopic analysis at the Institute of Geochemistry, Chinese Academy of Sciences (IGG-CAS) in Guangzhou, using a Neptune Plasma Multicollector-ICP-MS equipped with a 193 nm ArFexcimer laser ablation system. Procedures for analysis and calibration basically conformed to Wu *et al.* (2006). In order to achieve comprehensive and consistent data, we analysed Lu-Hf isotopes on identical zircon grains that had been implemented with O and U-Pb isotopic analyses, with an ablation pit radius of 60 μm , an ablation interval of 26 s for an individual measurement, and a repetition rate of 8 Hz at 10 J/cm². Normalisation to $^{179}\text{Hf}/^{177}\text{Hf} = 0.7325$ was conducted on the measured data. Zircon standard 91500 and Mud Tank were used for calibration. Analytical signals were selected and integrated offline using the ICPMSDataCal software, accompanied by mass bias calibration (Liu *et al.*, 2010). The data for reference materials are listed in Table S-5-5.

In situ zircon O isotopic measurement

Prior to measurements, high-purity gold was used to coat zircons in a vacuum environment using the Cameca IMS-1280 Secondary Ion Mass Spectrometry (SIMS) at the Institute of Geochemistry, Chinese Academy of Sciences (IGG-CAS), Guangzhou. Subsequently, we adopted multi-collection mode to measure oxygen isotopes. Our analytical procedures conformed to Li *et al.* (2010) and Tang *et al.* (2015). Normalisation to the Vienna Standard Mean Ocean Water composition (VSMOW, $^{18}\text{O}/^{16}\text{O} = 0.0020052$) was implemented on measured data. Subsequently, the Penglai zircon standard ($\delta^{18}\text{O} = 5.3 \text{ ‰}$, Li *et al.*, 2010) was used to calibrate the instrumental mass fractionation factor (IMF). Possible geometrical effects ('X-Y' effect) were avoided through mounting the standards to the close unknowns (Kita *et al.*, 2009; Tang *et al.*, 2015). The IMF veracity was validated by analysing another zircon standard (91500, mounted at the center) as an unknown, resulting in a weighted mean of $\delta^{18}\text{O} = 9.93 \pm 0.4 \text{ ‰}$ (2SD), which shared good consistency with that by Wiedenbeck *et al.*, (2004), namely 9.9 ‰. The data for reference materials are listed in Table S-5-6.



Supplementary Tables

Table S-1 Whole-rock Nd and Hf isotopic compositions of the granites from Kekeagashi, Tiemuerte, Jiaertasi, Chaganxile, and Sareshuoke plutons.

Sample	Age(Ma)	$^{147}\text{Sm}/^{144}\text{Nd}$ ^a	$^{143}\text{Nd}/^{144}\text{Nd}(\pm 2\sigma)$	$(^{143}\text{Nd}/^{144}\text{Nd})_i$	$\varepsilon_{\text{Nd}}(t)$ ^b	2σ	MSWD
Kekeagashi@01	409	0.1151	0.512189±6	0.512024	-4.6	0.1	14
Kekeagashi@02	409	0.1154	0.512175±8	0.512008	-4.9	0.2	
Kekeagashi@03	409	0.1156	0.512185±8	0.512018	-4.8	0.2	
Kekeagashi@04	409	0.1177	0.512151±6	0.511983	-5.5	0.1	
Tiemuerte@01	420	0.1427	0.512249±6	0.512046	-4.8	0.1	5.7
Tiemuerte@02	420	0.1318	0.512245±10	0.512053	-4.4	0.2	
Tiemuerte@03	420	0.1333	0.512231±10	0.512038	-4.7	0.2	
Tiemuerte@04	420	0.1355	0.512213±6	0.51202	-5.2	0.1	
Jiaertasi@01	425	0.1233	0.512261±10	0.512082	-3.6	0.2	7.3
Jiaertasi@02	425	0.1485	0.512276±6	0.512066	-4.6	0.1	
Jiaertasi@03	425	0.136	0.512268±8	0.512073	-4.1	0.2	
Jiaertasi@04	425	0.145	0.512278±8	0.512071	-4.4	0.2	
Chaganxile@01	430	0.1231	0.512178±8	0.512	-5.1	0.2	2.7
Chaganxile@02	430	0.1335	0.512182±10	0.511989	-5.6	0.2	
Chaganxile@03	430	0.1292	0.512161±10	0.511973	-5.8	0.2	
Chaganxile@04	430	0.1304	0.512185±6	0.512001	-5.3	0.1	
Sareshuoke@01	437	0.1281	0.512256±8	0.512072	-3.8	0.2	2.2
Sareshuoke@02	437	0.1266	0.512249±6	0.512068	-3.8	0.2	
Sareshuoke@03	437	0.1378	0.512271±6	0.512075	-4	0.2	
Sareshuoke@04	437	0.1268	0.512278±10	0.512093	-3.3	0.2	
Sample	Age(Ma)	$^{176}\text{Lu}/^{177}\text{Hf}$ ^c	$^{176}\text{Hf}/^{177}\text{Hf}(\pm 2\sigma)$	$(^{176}\text{Hf}/^{177}\text{Hf})_i$	$\varepsilon_{\text{Hf}}(t)$ ^d	2σ	MSWD
Kekeagashi@01	409	0.0297	0.282865±10	0.282637	4.2	0.4	2.8
Kekeagashi@02	409	0.0324	0.282897±10	0.282649	4.6	0.4	
Kekeagashi@03	409	0.03071	0.282879±9	0.282644	4.5	0.3	
Kekeagashi@04	409	0.03106	0.282869±8	0.282631	4	0.3	
Tiemuerte@01	420	0.02935	0.282890±10	0.282659	5.3	0.4	1.8
Tiemuerte@02	420	0.02851	0.282892±10	0.282668	5.6	0.4	
Tiemuerte@03	420	0.02953	0.282890±9	0.282658	5.2	0.3	
Tiemuerte@04	420	0.02851	0.282896±10	0.282672	5.7	0.4	
Jiaertasi@01	425	0.02851	0.282892±9	0.282665	5.6	0.3	3.8
Jiaertasi@02	425	0.02772	0.282869±9	0.282649	5	0.3	
Jiaertasi@03	425	0.02614	0.282868±10	0.282659	5.4	0.4	
Jiaertasi@04	425	0.02566	0.282854±8	0.28265	5	0.3	
Chaganxile@01	430	0.03326	0.282938±8	0.282669	5.8	0.3	3.9
Chaganxile@02	430	0.02772	0.282885±9	0.282662	5.6	0.3	
Chaganxile@03	430	0.0297	0.282923±8	0.282684	6.3	0.3	
Chaganxile@04	430	0.02851	0.282901±8	0.282671	5.9	0.3	
Sareshuoke@01	437	0.03019	0.282866±10	0.282619	4.2	0.4	2.4
Sareshuoke@02	437	0.0297	0.282853±9	0.28261	3.9	0.3	
Sareshuoke@03	437	0.03326	0.282895±9	0.282622	4.3	0.3	
Sareshuoke@04	437	0.03037	0.282856±9	0.282607	3.8	0.3	



Sareshuoke@04	0.047707	0.003986	0.001538	0.000039	0.282667	0.000015	5.06	-0.95	850	958
Sareshuoke@05	0.053616	0.004768	0.001657	0.000046	0.282652	0.000019	4.66	-0.95	866	979
Sareshuoke@06	0.039908	0.006017	0.001337	0.000044	0.282715	0.000024	6.68	-0.96	788	884
Sareshuoke@07	0.047113	0.001577	0.001336	0.000038	0.282673	0.000028	5.56	-0.96	831	939
Sareshuoke@08	0.038709	0.001438	0.001241	0.000044	0.282217	0.000029	-10.59	-0.96	1477	2080
Sareshuoke@09	0.041609	0.003623	0.001233	0.000037	0.282688	0.000016	5.94	-0.96	814	917
Sareshuoke@10	0.043915	0.004752	0.001347	0.000337	0.282712	0.000016	7.06	-0.96	774	866
Sareshuoke@11	0.127808	0.002511	0.003634	0.000038	0.282683	0.000026	5.30	-0.89	870	954
Sareshuoke@12	0.057513	0.003967	0.001739	0.000045	0.282784	0.000029	9.42	-0.95	682	745
Sareshuoke@13	0.072206	0.004749	0.002038	0.000045	0.282784	0.000016	9.33	-0.94	687	750
Sareshuoke@14	0.117314	0.002354	0.003441	0.000035	0.282716	0.000023	6.26	-0.90	820	899
Sareshuoke@15	0.091031	0.001598	0.002542	0.000039	0.282664	0.000018	5.02	-0.92	873	973
Sareshuoke@16	0.048802	0.001077	0.001339	0.000046	0.282197	0.000025	-11.33	-0.96	1509	2126
Sareshuoke@17	0.101907	0.000478	0.002941	0.000043	0.282778	0.000028	8.72	-0.91	719	781
Sareshuoke@18	0.088613	0.005945	0.002449	0.000034	0.282279	0.000023	-8.81	-0.93	1439	1679
Sareshuoke@19	0.127809	0.003734	0.003632	0.000032	0.282687	0.000027	5.34	-0.89	870	954
Sareshuoke@20	0.053913	0.003474	0.001831	0.000034	0.282688	0.000017	9.74	-0.95	669	729
Sample	$^{18}\text{O}/^{16}\text{O}$	1SE(%)	$\delta^{18}\text{O}(\text{‰})$	2SE(‰)	MSWD	[U]($\mu\text{g/g}$)	[Th] ($\mu\text{g/g}$)	Age(Ma)	σ	
Kekeagashi@01	0.002031	0.012	9.95	0.12	27	152.6	82.3	408	16	
Kekeagashi@02	0.002031	0.014	9.79	0.14		264.5	255.1	408.3	11	
Kekeagashi@03	0.002031	0.009	10.02	0.09		153.9	139.8	407.1	13	
Kekeagashi@04	0.002037	0.008	10.88	0.12		147.9	66.3	2159.6	37	
Kekeagashi@05	0.002025	0.011	9.53	0.11		250.7	82.8	408.6	15	
Kekeagashi@06	0.00203	0.013	10.23	0.12		212.6	63.5	2678.3	48	
Kekeagashi@07	0.002031	0.011	9.78	0.11		308.5	251.6	409.4	14	
Kekeagashi@08	0.002035	0.012	11.23	0.12		154	88.3	412.9	16	
Kekeagashi@09	0.002035	0.012	11.39	0.12		258.7	239.6	408.3	10	
Kekeagashi@10	0.002033	0.011	10.05	0.09		186.9	58.3	2930.7	39	
Kekeagashi@11	0.002031	0.011	9.86	0.11		157.2	94.2	410.5	12	
Kekeagashi@12	0.002031	0.012	10.16	0.12		248.5	81.8	410.1	15	
Kekeagashi@13	0.002033	0.009	11.02	0.09		121.8	78.7	408.3	11	
Kekeagashi@14	0.002031	0.02	10.1	0.2		314.4	255.2	407.7	14	
Kekeagashi@15	0.00203	0.01	9.5	0.1		152.5	75	407.3	17	
Kekeagashi@16	0.00203	0.01	9.55	0.1		178.1	94.5	409.4	12	
Kekeagashi@17	0.002032	0.011	10.02	0.12		158.3	119.8	410.6	11	
Kekeagashi@18	0.002031	0.014	9.98	0.14		161	99.3	408.4	12	
Kekeagashi@19	0.002032	0.015	10.23	0.15		251.9	81.8	408.2	15	
Kekeagashi@20	0.002031	0.008	9.88	0.08		128.5	84.6	413.8	13	
Tiemuerte@01	0.002029	0.011	11.64	0.11	17	537.2	179.5	421	14	
Tiemuerte@02	0.002031	0.011	10	0.11		421	358	424	14	
Tiemuerte@03	0.002033	0.011	9.98	0.12		225.7	86.9	3459.8	59	
Tiemuerte@04	0.002031	0.011	10.08	0.12		221.9	71.2	2930.1	48	
Tiemuerte@05	0.002032	0.013	9.75	0.13		166.7	83.8	418.5	11	
Tiemuerte@06	0.002032	0.012	9.77	0.12		477.8	427.3	421.4	17	



Tiemuerte@07	0.002032	0.012	9.99	0.12		118.5	100	421.7	14
Tiemuerte@08	0.002033	0.011	11.75	0.11		256.8	83.7	3255.7	40
Tiemuerte@09	0.002032	0.009	9.9	0.09		576.5	192.2	421.7	10
Tiemuerte@10	0.002032	0.009	9.83	0.09		428.7	377.4	417.9	12
Tiemuerte@11	0.002032	0.014	9.86	0.14		195.9	158.9	419.1	12
Tiemuerte@12	0.002034	0.013	10.62	0.13		165.8	85.1	418.2	12
Tiemuerte@13	0.002032	0.009	10.05	0.09		497.2	441.4	421.4	17
Tiemuerte@14	0.002032	0.01	9.89	0.1		119.2	97.5	422.4	17
Tiemuerte@15	0.002033	0.015	10.17	0.15		541.9	182.2	421.1	10
Tiemuerte@16	0.002031	0.015	11.62	0.16		267.3	68.1	1989.8	42
Tiemuerte@17	0.002032	0.012	9.93	0.12		203.5	168.7	424.2	12
Tiemuerte@18	0.002032	0.013	9.82	0.13		166.1	84	420	11
Tiemuerte@19	0.002033	0.016	10.19	0.16		491.5	442.4	419.5	18
Tiemuerte@20	0.002033	0.015	10.35	0.15		119.8	99.2	423.3	16
Jiaertasi@01	0.002034	0.011	10.78	0.11		458.2	263.7	425.6	12
Jiaertasi@02	0.002033	0.01	10.11	0.1		817	567.9	423.8	13
Jiaertasi@03	0.002032	0.007	9.65	0.07		510.5	392.6	424	11
Jiaertasi@04	0.002032	0.013	9.84	0.13		503	294.8	419.8	16
Jiaertasi@05	0.002033	0.012	10.18	0.12		603.2	502.8	426.1	14
Jiaertasi@06	0.002031	0.012	9.54	0.12		858	479.9	424.2	14
Jiaertasi@07	0.002031	0.023	9.41	0.23		466.3	266.8	425.9	14
Jiaertasi@08	0.002033	0.023	10.38	0.23		802.7	540.9	424.7	14
Jiaertasi@09	0.002031	0.013	9.6	0.13		528.1	417.4	428.5	14
Jiaertasi@10	0.002033	0.012	9.65	0.12	14	285.6	152.3	3103.8	41
Jiaertasi@11	0.002028	0.011	11.01	0.11		514.8	306.4	424.9	15
Jiaertasi@12	0.002032	0.016	9.72	0.16		593.3	485.1	424.5	19
Jiaertasi@13	0.002033	0.012	10.27	0.12		706.7	362.6	427.4	18
Jiaertasi@14	0.002033	0.014	10.17	0.14		453.1	261.6	427.5	13
Jiaertasi@15	0.002033	0.007	10.46	0.07		804.5	553.1	428.4	13
Jiaertasi@16	0.002032	0.017	9.8	0.17		521.5	406.7	425.2	12
Jiaertasi@17	0.00203	0.011	9.31	0.16		373.6	105.5	2306.7	31
Jiaertasi@18	0.002032	0.011	10.01	0.11		499.9	294	428.4	16
Jiaertasi@19	0.002033	0.009	10.13	0.09		603.7	503.1	426	16
Jiaertasi@20	0.002032	0.009	9.88	0.09		754.1	400.3	424.1	16
Chaganxile@01	0.002032	0.011	9.76	0.11		688.6	457.2	430.2	7
Chaganxile@02	0.002032	0.012	10.09	0.12		486.5	113	430.2	20
Chaganxile@03	0.002031	0.016	9.59	0.16		2331.5	885.5	430.5	6
Chaganxile@04	0.00203	0.015	10.46	0.13		984.3	331.6	2987.3	36
Chaganxile@05	0.002033	0.013	10.22	0.15		549.3	238.1	3505.7	43
Chaganxile@06	0.002032	0.012	10.04	0.12	16	1484.2	804.9	430.2	11
Chaganxile@07	0.002033	0.014	10.21	0.14		145.3	66.6	430.4	10
Chaganxile@08	0.002033	0.012	10.42	0.12		540	172.7	429.2	8
Chaganxile@09	0.002033	0.019	10.25	0.19		522.2	153	431	9
Chaganxile@10	0.002032	0.018	10.11	0.15		563.7	369.2	430.9	8
Chaganxile@11	0.002033	0.013	10.16	0.13		2613.3	1062.9	430.4	5



Chaganxile@12	0.002033	0.013	10.44	0.13		1538.7	842.2	430.3	18
Chaganxile@13	0.002032	0.011	9.89	0.11		167.6	86.4	430.3	10
Chaganxile@14	0.002031	0.016	9.18	0.16		496.2	152.5	430	7
Chaganxile@15	0.002025	0.012	9.57	0.12		519.6	155.6	431.4	8
Chaganxile@16	0.002028	0.009	10.96	0.09		619.1	416.4	430.4	7
Chaganxile@17	0.002032	0.012	9.99	0.12		2629.9	1054.1	430.7	4
Chaganxile@18	0.002025	0.008	9.54	0.08		1473.3	832.2	430.8	19
Chaganxile@19	0.002033	0.014	10.3	0.14		172.1	92.9	430.8	8
Chaganxile@20	0.002025	0.007	9.56	0.07		467.1	142.7	430	6
Sareshuoke@01	0.002026	0.01	10.1	0.1		572.7	255.4	436.5	12
Sareshuoke@02	0.002026	0.013	9.7	0.13		647.6	480.4	437.7	9
Sareshuoke@03	0.002031	0.013	9.44	0.13		867.3	512.2	439.1	10
Sareshuoke@04	0.002025	0.013	9.48	0.13		506.8	258	437.3	18
Sareshuoke@05	0.002026	0.01	9.63	0.1		1378.9	1176	435.9	8
Sareshuoke@06	0.002025	0.009	9.57	0.09		1029.3	637.2	436.4	13
Sareshuoke@07	0.002026	0.01	10.09	0.1		567.7	256.7	437.5	15
Sareshuoke@08	0.002024	0.008	9.58	0.12		651.1	204.9	2625.3	38
Sareshuoke@09	0.002025	0.009	9.45	0.09		667.8	488.2	437.1	9
Sareshuoke@10	0.002026	0.012	9.62	0.12	12	884.8	531.2	440.5	12
Sareshuoke@11	0.002025	0.016	9.46	0.16		478.5	226.4	440.9	23
Sareshuoke@12	0.002026	0.014	10.06	0.14		1181.1	973.8	441.4	15
Sareshuoke@13	0.002025	0.01	9.42	0.1		1019.6	649.9	439	18
Sareshuoke@14	0.002025	0.011	9.57	0.11		570.8	255.1	437.4	13
Sareshuoke@15	0.002032	0.011	10.48	0.11		662.9	478.4	437.7	10
Sareshuoke@16	0.002031	0.012	9.38	0.12		682.9	223.3	2857.9	36
Sareshuoke@17	0.002026	0.016	9.8	0.16		880.3	519.2	438.2	10
Sareshuoke@18	0.002035	0.013	11.12	0.13		697.2	129.7	3043.6	20
Sareshuoke@19	0.002034	0.013	10.85	0.13		1217.2	1002.6	437.8	13
Sareshuoke@20	0.00203	0.012	9.45	0.12		1023.6	643.5	437.3	16

Table S-3 Global compilation of published Hf and Nd isotopic compositions of A-type granites.

Reference	Sample number	Mean value of $\epsilon_{\text{Nd}}(t)$	Sample number	Mean value of $\epsilon_{\text{Hf}}(t)$
Niu <i>et al.</i> , 2011	DZZ1-DZZ6	-16.833	DZZ3	-15.102
Luo <i>et al.</i> , 2018	L63-L68	2.243	L64	4.4
	L42-L46	-1.4	L42	2.9
Yang <i>et al.</i> , 2006	JH-07-JH30	-13.85	03JH029-40	-13.344
	FW01-162-FW01-164	-13.55	FW01-162	-11.985
Zhang <i>et al.</i> , 2013	09KZ01-09KZ04	-1.467	09KZ05	0.915
	09GL01-10	-0.178	09GL07	1.431
	09HLJ V-1-9	0.1025	2010 HLJ III-V, 08KT01, HLJ026-28	0.379
Zheng <i>et al.</i> , 2017a	ZK1902-Y-8-ZK3204-Y-2	-5.514	ZK1902-Y-7 -ZK2805-Y	0.811
Yan <i>et al.</i> , 2018	15SJW-1-15SJW-5	-4.53	15SJW	0.792
Zhao <i>et al.</i> , 2015a	BSS-2-BSS-8	-3.575	BSS-4-BSS8	0.164
	12JGS-3-12JGS-5	-3.3	12JGS-5	-1.026



	12WS-1-12WS-4	-4.125	12WS-1-12WS-4	-1.473
Yang <i>et al.</i> , 2012	XL-5-XL17	-4.678823529	XL-11	-4.738
	DQW-1-DQW-3	-5.36		
Chen <i>et al.</i> , 2015b	BZS-1-BZS-6	-11.733	BZS4-BZS5	-7.661
	DMS-1	-11.2	DMS-1-DMS-19	-7.726
Cai <i>et al.</i> , 2017	X3-X7	-1.754	X3-X5	-1.923
Feng <i>et al.</i> , 2014	09HT-1-09HT-10	-9.257	HT-9a	-8.054
	09EP-1-09EP-4	-8.133	EP-4	-6.639
	09HT-9b	-7.3	HT-9b	-8.036
Zhao <i>et al.</i> , 2013	08TS-09TS	-9.667	08TS-48	-7.509
	08GX-20-08GX-25	-13.8	08GX-20-08GX-24	-11.915
Zhang <i>et al.</i> , 2014	BYH-10	4.835	BYH1	9.76
Chen <i>et al.</i> , 2015c	LLS2-LLS8	-11.65	LLS2-LLS6	-9.61
Hu <i>et al.</i> , 2017	13ZJ26-13ZJ89	-3	13ZJ28-13ZJ89	-1.353
Li <i>et al.</i> , 2018a	12WN-12-12WN-16	-1.967	12WN-12-12WN-16	6.623
Li <i>et al.</i> , 2018b	HC1-HC23	-4.86	HC4-17	-7.025
Sun <i>et al.</i> , 2017	8047-8052	-9.325	08047	-8.688
	8041-8045	-9.36	08042	-7.627
Zhao <i>et al.</i> , 2009	SC7-SC15,DF9-DF-11	-7.36	DF-43	-11.656
	SC11,DF33-DF38	-6.85	DF-38	-8.536
Zhou <i>et al.</i> , 2015a	12ZX11-12ZX17	0.265	12ZX13	-0.44
Shen <i>et al.</i> , 2011	08WLG13-08WLG17	5.65	08WLG07-08WLG16	14.027
	08QH24-08QH29	7.12	08QH25-08QG27	11.688
Zhao <i>et al.</i> , 2008	KD06-32-KD06-189	0.971	KD06-32-KD06-157	6.817
Gu <i>et al.</i> , 2017	13CZYS-02-13CZYS-10	-6.053	13CZYS02-13CZYS08	-3.293
Deng <i>et al.</i> , 2016	GJY6-GJY22	-5.713	GJY6-GJY22	-9.018
Wang <i>et al.</i> , 2013a	DYC14-DYC38	-9.316	DYC12-DYC36	-6.883
Xia <i>et al.</i> , 2012	JLH03-JLH06	-4.967	JLH03	-8.76
	JJ03-JJ07	-7.025	JJ03-JJ07	-11.645
Sun <i>et al.</i> , 2011	LS12-LS15	-13.5	LS15	-14.294
Jiang <i>et al.</i> , 2011	TS1-TS9	-3.75	TS-4	-3.9
	DMS1-DMS16	-3.206	DMS2-DMS9	-2.364
	TS-4-2	0.9	TS-4-2	-6.163
Zhou <i>et al.</i> , 2012	HG1-HG3	0.033	HG1-HG3	6.908
Zhou <i>et al.</i> , 2015b	ZK10C02-ZK14B04	-8.691	HG-3-5-20	-9.111
Wang <i>et al.</i> , 2010	LG78-LG88	4.608	17.1	12.515
Xin <i>et al.</i> , 2018	JCHGY-Y1-JCHGY-Y7	-3.456	XTB-2016-N1-XTB-2016-N2	1.510
Jiang <i>et al.</i> , 2018b	JHS01-JHS21	-6.747	JHS01-JHS21	5.571
Zhou <i>et al.</i> , 2017	12ZX03-12ZX08	-10.988	12ZX03	-17.764
Xia <i>et al.</i> , 2016	MH01-MH23	-2.86	MH01-MH23	-3.392
	SH03-SH06	-0.9	SH03	-6.491
Zhao <i>et al.</i> , 2016a	ZJJ3-ZJJ6	-7.45	ZJJ-3	-7.25
	ZJJ8-ZJJ11	-6	ZJJ-8	-4.690
	12THD-1-12THD-4	-6.15	12THD-1-12THD-4	-4.271
	XZD1-XZD10	-6.15	XZD-2	-4.305



Jiang <i>et al.</i> , 2017	HMG01-HMG08	-11	HMG06	-11.8
	TPL06-TPL09	-11.05	TPL07	-10.925
Chen <i>et al.</i> , 2016b	DL-500-DL-640	-8.548	DL-500-DL-640	-10.537
Zheng <i>et al.</i> , 2017b	XS-Y-1-XS-Y-4	-6.65	XS-Y-6	-2.528
Gürsu <i>et al.</i> , 2018	DPK17A-DPK72	-4.25	Z17A-DPK27-DPK72	-0.016
Zhou <i>et al.</i> , 2018	1-18	-6.043	1-18	-0.011
	PT03-PT04	-2.213	PT03-PT04	-0.8
Zhang <i>et al.</i> , 2018b	Taerbaха-01-Taerbaха-04	4.795	Taerbaха	9.963
	KujibeiEa-KujibeiEb	4.636	KujibeiEa-KujibeiEb	9.813
	Qibaertie-01-Qibaertie-04	5.2	Qibaertie	10.404
	WuerkashierN-01-WuerkashierN-04	7.73	WuerkashierN	13.705
	WuerkashierE-01-WuerkashierE-04	5.583	WuerkashierE	10.912
	HebukesairSW-01-HebukesairSW-04	8.033	HebukesairSW	14.755
	HebukesairN-01-HebukesairN-04	8.105	HebukesairN	15.218
Cao <i>et al.</i> , 2014	G1	-7.5	G1	-4.42
Li <i>et al.</i> , 2018a	XHL5-XHL7	-6.171	XHL5-XHL7	-7.254
Wang <i>et al.</i> , 2015a	13FRS-14-13FRS-20	-3.475	13FRS-12-13FRS-15	0.791
Li <i>et al.</i> , 2018b	Qitianling	-6.59	Qitianling	1.5
	Qianlishan	-6.7775	Qianlishan	2
	Jinjiling	-7.475	Jinjiling	2
	Tongshanling	-4.7	Tongshanling	1.5
	Baoshan	-6.3	Baoshan	1.5
	Xihuashan	-10.7925	Xihuashan	2.5
	Guposhan	-3.783333333	Guposhan	1.5
	Huashan	-3.523333333	Huashan	1
	Huangshaping	-5.233333333	Huangshaping	2
	Hehuaping	-6.52	Hehuaping	1.5
Gao <i>et al.</i> , 2016	ZK702-ZK804	-14.575	119	-14.9
Ye <i>et al.</i> , 2016	13TR02	-3.017	13TR01-12TR07	-2.114
Zhang <i>et al.</i> , 2017d	XS1507-XS1530	-4.967	XS1507-XS1530	-2.576
Wang <i>et al.</i> , 2017	1504FY3	-6.2	1403FY13-5	-0.3
	1410SMS1-1410SMS4	-2.225	07SMS	-0.61
Lan <i>et al.</i> , 2015	CY2-49-CY2-92	-4.633	CY2-92	-5.573
	CY2-43-CY2-44	-4.5	CY2-43	-4.235
Zhong <i>et al.</i> , 2017	13ts14B-13ts14I	-1.255	13ts14B-13ts14I	3.039
Ding <i>et al.</i> , 2014	BLGTC104-B1-BLGTC104-B11	-3.3	BLG-TC104-B1-BLGTC104-B9	-1.497
	XI01-X102	-5.333	XI01-X102	-3.05
Zhu <i>et al.</i> , 2016	HCQ1003-HCQ1308	-0.335	HCQ1003	8.792
	KMZ1001-KMZ1103	-5.82	KMZ1001	1.056
Li <i>et al.</i> , 2015c	11QJ5-10QJ-3D	4.3	10QJ-3D	13.143
Chen <i>et al.</i> , 2013a	KH128-KH174	-0.675	KH128-KH174	1.889
Su <i>et al.</i> , 2013	FC2	-8.4	FC2	-8.732
	HS5	-5	HS5	-2.735
Tang <i>et al.</i> , 2010	06XJ017-06XJ23-2	-1.502	06XJ17	4.105
	06XJ04-06XJ15	0.126	06XJ13	5.333



Hu <i>et al.</i> , 2016	YNG12	-2.403	YNG1201	-3.35
	QMX12	-3.713	QMX12	-3.71
	DL09	-3.01	DL09	-2.355
Liu <i>et al.</i> , 2008	JX1-JX10	-18.733	JXZ01-JXZ19	-23.732
	WL2-WL12	-19	WLZ01-WLZ17	-23.724
Guo <i>et al.</i> , 2012	XHS3-XHS35	-10.72	XHS-4	-10.218
	X09,XHS1-24	-11.02	XHS-22	-10.047
	XHS15-XHS37	-10.85	XHS15-XHS37	-10.367

Table S-3 (continued). Global compilation of published Hf and Nd isotopic compositions of I-type granites.

Reference	Sample number	Mean value of $\epsilon_{\text{Nd}}(t)$	Sample number	Mean value of $\epsilon_{\text{Hf}}(t)$
Yan <i>et al.</i> , 2017	TXH1-TXH4	-4.997	TXH-1	-4.382
Konopelko <i>et al.</i> , 2018	4-17	-4.800	04-11	-0.054
Yang <i>et al.</i> , 2017	DY001-DY006	-6.651	DY002	-8.480
	JZ001-JZ006	-5.799	JZ006	-5.433
Qiu <i>et al.</i> , 2017	HC2-HC7	-9.160	HC1	-11.272
Jiang <i>et al.</i> , 2018a	G1,ZK301.4-ZK301.9	-11.867	ZK301-4	-11.881
	G2,340.13-340.30,ZK301.1,ZK301.3	-11.714	340-13	-11.444
Yu <i>et al.</i> , 2017	KN01-KN04	-0.567	KN01-KN04	5.133
	ALT66-ALT67	0.600	ALT66-ALT67	11.500
	ALT03-ALT04	-0.250	ALT03-ALT04	5.450
	ALT15-ALT17	-1.267	ALT15-ALT17	5.067
	HM02-HM12	-2.725	HM02-HM12	4.250
	KW14-KW16	-0.567	KW14-KW16	3.733
	JDY13-JDY15	-1.133	JDY13-JDY15	9.233
Li <i>et al.</i> , 2015b	AG1-AG10,ABG1-ABG2,AGM1	7.455	ABG1-AGM1	11.183
Zhou <i>et al.</i> , 2011	XT4-XT12,LJG1-LJG9	2.540	XT3	8.115
Luo <i>et al.</i> , 2018	L49-L52	0.050	L52	7.650
	L53-L57	-3.500	L53	-0.150
	L37-L41	1.960	L38	7.850
Zhao <i>et al.</i> , 2018	RJ01-RJ09	0.863	RJ01	6.573
Zhu <i>et al.</i> , 2011	LiN2-LiN6	-6.340	LiN4	-3.356
	LuN1-LuN2	-5.250	LuN1	-2.800
	BW1-BW6	-6.067	BW1	-0.230
He <i>et al.</i> , 2018a	BMXS1-BMXS12	-6.323	BMXS1,BMXS10	-2.438
Li <i>et al.</i> , 2016a	EK4.1-EK4.2,Zh1.1	1.567	EK4.2,Zh1.1	10.810
	Zh2.10-Zh5	0.800	Zh2.1	6.853
	Ash2-Ash5	0.650	Ash-5	9.681
Deng <i>et al.</i> , 2018	SK45-SK77	3.850	SK76	7.595
Cao <i>et al.</i> , 2014	G21-G23	-13.833	G21	-9.636
Yu <i>et al.</i> , 2016	XQ10.1-XQ10.13	-9.550	XQ10.3	-8.571
	XQ10.11-XQ10.15	-8.000	XQ10.15	-6.244
Zhang <i>et al.</i> , 2017e	12JH160-12JH243	-10.637		-10.937
Cao <i>et al.</i> , 2017	10BSD9-10BSD12, BSD01*-BSD02*	5.180	BSD9,BSD13	7.575



	BS16-BS17,BSZK15-5-405	5.767	BS-16	6.767
Wang <i>et al.</i> , 2017	KFP2-KFP10	-1.233	KFP4	-5.278
Jia <i>et al.</i> , 2018	SGS01.1-SGS01.3,AM01-1	-3.293	AM01,SGS02	0.149
	WC01.1-WC01.2	-3.290	WC01	0.396
	SR04.1-SR04.3	-3.873	SR04	-0.425
Gao <i>et al.</i> , 2014b	TSM1-TSM60	-11.667	TSM20	-13.000
	TQG1-TQG6,13TQG1-13TQG6	-3.500	TQG1	4.150
Zhou <i>et al.</i> , 2017	12WW08-12WW76	2.090	12WW15,12WW52	4.456
Wu <i>et al.</i> , 2017	SCM11h-SCM16h	-4.067	SCM10	-0.839
	JDC2H-JDC3H,CJM2-CJM9	-6.950	JDC2	-1.692
	HZS1H-HZS15H	-8.000	HZS8	-8.550
Liu <i>et al.</i> , 2017	13ZJS10-13ZJS18	-5.480	13ZJS14	-5.445
	13ZJS10.1-13ZJS18.1	-5.323	13ZJS16.1	-5.128
Karsli <i>et al.</i> , 2016	CM6-CM19	-4.580	CM21	-1.800
	CS5-CS10	-3.975	CS10	0.220
He <i>et al.</i> , 2018b	ZK0810.1-ZK0814.1	-4.648	ZK0810.1,ZK0813.1	-4.254
Zhong <i>et al.</i> , 2011	ALH-0702,ALH-0401	-6.630	ALH-0401,ALH-0702	-2.218
Qin <i>et al.</i> , 2009	MG02,MG08	-6.385	MG01-MG29	0.995
	ME23,ME26	-6.500	ME03-ME19	1.102
Yuan <i>et al.</i> , 2016	EL10.9.1-EL10.9.8	4.025	EL10.9.1	11.383
	EL10.6.1-EL10.6.2	2.150	EL10.6.5	9.847
	9HS16.1-9HS16.2,9HS15.3.2,9HS15.6.1	1.100	9HS16-2,9HS15.3.2	6.890
Xia <i>et al.</i> , 2017	13NGT01.1-13NGT01.12	-12.067	13NGT12.1	-1.200
Moghadam <i>et al.</i> , 2015	K12-3,K12-23	-1.637	KR12	3.172
Yang <i>et al.</i> , 2016a	HNDSTB3-HNDSTB4,HNBY8	-6.233	HNDSTB3,HNDSTB4	-5.558
	HZK0906B24-HZK0906B33	-7.317	HZK0906B29	-5.733
Mao <i>et al.</i> , 2017	YCLB1-YCLB32	-5.300		-1.803
Chen <i>et al.</i> , 2014	08JH256-08JH272	-1.271	MG	3.600
Wang <i>et al.</i> , 2015c	WR12.40-WR12.48	-0.580	WR12	6.728
Wang <i>et al.</i> , 2014b	XWC11.01-XWC11.33,SXWC10-04-SXWC10-45	-7.600	XWC11	-5.497
	RL12.01,RL12.08,HS12.05	-7.733	RL11,HS10	-7.070
	TCG12.05,TCG12.10	-5.450	TCG11.01	-4.654
Wang <i>et al.</i> , 2015b	WT2-WT6	-15.840	WT3	-20.657
	WT7-WT13	-13.733	WT13	-16.329
	SP4-SP9	-14.520	SP7	-15.684
	SP1-SP3	-8.633	SP2	-6.912
	WT1-WT15	-12.550	WT9	-10.865
Zhang <i>et al.</i> , 2015	BL004-BL009	2.860	BL004	5.140
	BL050-BL065	5.207	BL050.1-BL065.24	10.470
Zhou <i>et al.</i> , 2015b	TBD05-TBD10	-1.980	TBD-05	6.631
	TBD09-TBD14	-1.740	TBD-12	2.184
Li <i>et al.</i> , 2013	B80628-8.2,DDQ09824-1.1-DDQ09824-2.1	-0.733	B80628-8.2.1-15,DDQ09824-1.1.1-13-DDQ09824-2.1.1-13	4.324
Dan <i>et al.</i> , 2016	09AL147-09AL148	-8.400	09AL147	-6.817



Song <i>et al.</i> , 2018b	DST1-DST3	3.867	DST1	-1.678
Yang <i>et al.</i> , 2016b	SKS6-SKS50	-6.025	SKS31,SKS36	-8.865
Li <i>et al.</i> , 2015a	TR1.5-TR1.8	-7.733	TR1.1	-2.579
	TR2.1-TR2.3	-7.600	TR2.3	-3.123
Liu <i>et al.</i> , 2013	MC1.1,MC4	-2.800	MC1	0.275
Ma <i>et al.</i> , 2013	JJLL2-JJLL10	-19.031	JJLL1-JJLL6	-13.596
Gao <i>et al.</i> , 2017	RLB3-RLB9	-6.525	RL-B3,RL-B9	-5.973
	RLZK0002B7-RLZK0002B26	-7.200	RLZK20002B20	-5.800
Zi <i>et al.</i> , 2012	SJ110,SJ143	-7.130	SJ143	-9.856
Chen <i>et al.</i> , 2015a	YC1203-YC1211	-17.267	YC1204	-23.388
Zhang <i>et al.</i> , 2016	AHg01-AHg13	-7.050	AHG13	-5.098
Dan <i>et al.</i> , 2014	09AL10-09AL42	-11.705	09AL22,09AL27	-9.947
	09AL33-09AL38	-14.100	09AL33,09AL37	-11.523
He <i>et al.</i> , 2013	DC0901-DC0923	-7.213	DC0910,DC0922	-4.897
	XC0902-XC0905	-6.000	XC0903	2.013
Zhang <i>et al.</i> , 2008	04YC02,04YC05	-9.250	04YC02.1-04YC05.15	-9.200
	04YC11,04YC20	-8.100	04YC11	-11.107
	05XF08-05XF24	-8.475	05XF23	-12.471
Chen <i>et al.</i> , 2017b	XITG12-XITG29	-7.270	XITG23,XITG27	-3.586
Nabatian <i>et al.</i> , 2016	GNTO1-GNTO81	1.704	GNTO1,GNTO2,GNT12	4.097
	GNTO02-GNTO33	1.970	GNTO33	3.778
	GNTO3-GNTO5	0.897	GNTO4	1.721
	GNTO6-GNTO49	1.213	GNTO47	3.160
Wang <i>et al.</i> , 2015d	09GS28,10GS08-10GS93	-0.033	09GS28,10GS93	0.132
Li <i>et al.</i> , 2015d	J11-5-2,J11-5-2R	4.850	J11-5-1	6.642
Gao <i>et al.</i> , 2014c	FN46-FN161	-13.127	FN46,FN63,FN89,FN126	-9.441
Yin <i>et al.</i> , 2017	WJ1126.1-WJ1126.3,WJ1136.1-WJ1136.3	5.309	WJ1126,WJ1136	13.243
Chen <i>et al.</i> , 2016a	C14.1-C14.3,CG72-CG81,HKAM168-HKAM182	2.625	CG71,CG79	9.575
Liu <i>et al.</i> , 2012	YSH01.1-YSH01.5	-0.967	YSH01.1	3.006
Wang <i>et al.</i> , 2014a	JHH,GHH1	-12.850		-16.100
Liu <i>et al.</i> , 2009	PH5.4,PH5.7,PH4.6,PH4.7,PH3.1,PH3.7,XD1,XD6,P DX4,PDX16	-9.560	PDXZ01,XDZ01,PHZ01	-11.473
Li <i>et al.</i> , 2007	2KSC3-2KSC79,P1-P9	-9.050	2KSC3,2KSC79	
	2KF396-2KF403	-6.233	2KF405	-8.753
	MR28,MR42	-6.100	MR42	-5.513
	2KG4.1-2KG4.4	-7.575	2KG1.3	-1.405
Ma <i>et al.</i> , 2014	DX66A-DX-66F	-1.780	DX66B,DX66D	5.127
	DX57,DX59A	-1.400	DX57-DX58	4.133
Zhong <i>et al.</i> , 2013	J03161-J03162,FD05-FD09,FD11.1	-5.125	J03162	0.465
Xiao <i>et al.</i> , 2017	11LY1.1-11LY1.20	-3.455	11LY1.18	0.908
	11XY1.6-11XY1.7	-4.475	11XY1.6	0.952
	11JK1.2,11JK1.4	-3.515	11JK1.2	-3.713



	11NS1.1-11NS1.2	-5.695	11NS1.2	-3.947
Liao <i>et al.</i> , 2018	SK14.02-SK14.15	3.209	SK14.02-SK14.15	13.799
Qian <i>et al.</i> , 2017	TS-7-1	-0.600		8.150
	TS-14-1	-1.200		9.050
Dong <i>et al.</i> , 2018	SSWM5.1-SSWM5.4	-5.825	SSWM5.1	-5.175
	SSWM4.1-SSWM4.12	-4.450	SSWM4.1	-2.077
Bao <i>et al.</i> , 2018	ZS23-ZS41	-3.233	ZS21,ZS26,ZS34	-0.742
Chen <i>et al.</i> , 2013b	08JH332,08JH332,10JH184	-3.600	08JH332	-2.299
	08JH310,10JH189	-3.700	08JH308	-0.713
Cao <i>et al.</i> , 2016	ZK603.146,ZK403,360,BE2.0,ZK205.82,BHS	6.780	ZK003.233,BHS,BTC196	13.944
	ZK403.175,ZK603.116	7.100	BXS	14.239
Zhou <i>et al.</i> , 2018	13GD14.1,14GD10-14GD12	1.318	13GD14.1	11.183
Zhao <i>et al.</i> , 2012	Q93102-Q93106	-16.775	Q93105,LT28	-11.584
	Q93108.1-Q93108.6,LN05-LN18,LNS01-LNS16	-15.385	M0602,LN05	-21.696
	B0001.7,B0003.9,B2101.11,ZK001	-20.640	ZK0001	-29.311
	JD11-JD14	-15.333	JD23	-15.031
	JDC7-JDC100	-15.300	JDC34	-17.835
	sjwb1,sjwb2	-15.400	sj1	-17.959
	Q93109.1-Q93109.7,LF01-LF04	-17.950	LF04,HS10	-20.188
	HS6,HS9	-17.100	HSB1,HSB6	-22.359
	W2-W7	-12.900	WY15,W4	-11.853
	N1-N9	-16.183	NN18,N3,N6	-22.830
	MLG01,MLG06	-18.450	MLG06	-26.280
	LW01,HYY01 -HYY03	-10.300		-18.650
	LB01,LB03,LSB10-LSB92	-18.027	LSB43,LSB46,LSB47	-21.236
	LN1-LN4	-14.550	QYG16-5 19,LN3	-20.850
	YH108-YH146,43294-43297	-14.080	YH-110,07.15,07.16	-17.993
	Q9304.1-Q9304.7,HY01-HY60	-14.582	HY02,HY14,HY74,HY73,HY0701,HY070 2,YCL.1	-16.194
	07DG02,07DG06	-15.300	DG2,DG5,DG0908	-13.980
	RY09.1-RY09.7,RY0907a,RY0907b	-14.263	RY0709	-14.170
	TSM1-TSM60	-12.200	TSM31,TSM20	-12.163
	LHK1307.1-LHK1307.51	-12.825	LHK 1307	-11.905
	Q9401,Q9402,FN37-FN161	-14.036	FN46,FN63,FN89,FN126	-9.402
	Mh16,Mh9,09392.1-09392.8,9396,93101	-10.167	Q93101,MHG30	-10.545
	Xigou	-10.400	XG01,GG06	-4.992
	ML17,ML21	-4.200	09CL260,ML28/1B, ML32/1B	-9.169
	Q9308.1-Q9308.9,Q9309,L01-L09	-4.725	LJSB1,LJSB8	0.074
	101-3,CG3-CG8,SG20,201-58,201-60,101-25,1301-40	-5.240	CG2	-1.136



Table S-3 (continued). Global compilation of published Hf and Nd isotopic compositions of S-type granites.

Reference	Sample number	Mean value of $\epsilon_{\text{Nd}}(t)$	Sample number	Mean value of $\epsilon_{\text{Hf}}(t)$
Zhao et.al., 2017a	MON-37	0.800	MON37	5.207
	MON-60	1.850	MON-60	7.564
	MON-65	-0.433	MON65	3.925
Li et al., 2016b	NL1-NL13	-12.350	NL1-NL12	-12.265
Dan et al., 2014	09AL225-09AL233	-0.160	09AL233	1.133
	09AL258-09AL262	-0.043	09AL258	4.871
Zhang et al., 2017b	B2068-B2138	-1.250	B2127	0.824
Chen et al., 2017a	L13JP-21-L13JP-29	-4.975	L13JP-20	-2.747
	L13JP-37-L13JP-46	-4.767	L13JP-40	-2.490
	L13TC-02-L13TC-05	-6.700	L13TC-1	-2.986
Feng et al., 2018	Shimensi	-6.525		-6.150
	Pengshan	-5.890		-2.500
Qin et al., 2014	10QL151-10QL158	-9.380	10QL151	-7.312
Wu et al., 2017	AJSD-1h-AJSD-3h	1.545	AJSD-1-1-AJSD-1-12	-7.514
Zhang et al., 2018a	Wukuli-1-Wukuli-4	-3.550	Wukuli-1-Wukuli-15	-1.933
	Kadelat-1-Kadelat-4	-3.575	Kadelat-1-Kadelat-15	-3.879
	Aketas-1-Aketas-6	5.233	Aketas-1-Aketas-15	12.364
Zheng et al., 2018	BS-18-BS-30	-5.140	BS-18-02-BS-18-28	-0.630
	BH-16-BH-26	-5.090	BH-24-01-BH-24-32	-2.085
Peng et al., 2015	11ST-60C-11ST-61C	-10.938	11ST-60F	-11.206
Wang et al., 2013b	10DX-43a-10DX-45d	-6.800		-4.788
	10DX-85-10DX-90	-8.100		-9.950
	11ML-73-11ML-77	-6.800		-3.783
Hu et al., 2015	GE08191-GE08195	-6.950	GE08191,GE08195	-5.642
	BS08031-BS08034,BS1001-BS1005,BS0715	-6.588	BS08031,BS08034	-5.146
Liu et al., 2015	HH-43A-HH-45A,ML-34A-ML-34G	-9.875		-8.163
Wang et al., 2016	14XZ2.1,14NX3	-9.950	14NX3-2,14XZ2.1-3	-4.610
Guo et al., 2018	JLN-22,JLN-25	-10.200	JLN-22-3-JLN-22-27	-12.093
	DYL801-36-1-DYL801-160-1	-10.167	DYL801-36-2-1-DYL801-36-2-24	-11.959
	JLN-1,JLN-13	-10.700	JLN-11-1-JLN-11-37	-11.328
	JLN-6,JLN-16	-9.800	JLN-15-2-JLN-15-40	-9.530
Huang et al., 2014	81#-12-81#-26,ZK0-26-1-ZK0-26-3,ZK-1-4-ZK-1-13	-7.516	ZK-26-3-81#-23	-5.655
Zheng et al., 2008	03WN58-03WN73	-2.123	03WN71 ,03WN73	3.958
	03WN60- 03WN70	0.002	03WN61,03WN65	5.378
Zhang et al., 2017a	Plutons-Keketale	-2.547		2.294
Zhao et al., 2015b	10SC07A,10SC10	-8.850	10SC07A	-7.495
	10SC06A	-8.9	10SC06A	-9.224
	10SC01A,10SC05A	-11.000	10SC05A	-10.356
	10SC01N	-10.500	10SC04A	-10.210
Cheng et al., 2017	MZ13-3-MZ13-4	-12.720	MZ13-3	-4.326
	MZ13-7-MZ13-14	-12.133	MZ13-7	-4.551



Zhu <i>et al.</i> , 2009	PK01-1-PK01-6	-6.150	PK01-1	5.180
Martínez <i>et al.</i> , 2014	110217-110219	-6.657	106820	5.533
	110210-111383	-4.855	110210	5.075
	110331	-6.350	110331	2.400
	110341	-6.200	110341	-6.267
Wu <i>et al.</i> , 2006	03WN15- 03WN31	-0.523		5.400
	03WN01- 03WN13	-1.338		3.400
	03WN33- 03WN51	-0.758		3.500
Huang <i>et al.</i> , 2015	QL09-02-QL09-18	-4.350		0.775
Li <i>et al.</i> , 2015b	SH-04-SH-43,YJ-3-1	-9.840	SH-04,SH-29-A,YJ-3,YJ-3	-7.328
Gou <i>et al.</i> , 2015	W8011 -W8053	-6.780	W8011-W8017	-2.414
Xu <i>et al.</i> , 2015	13MG-11-13MG-14	-11.685	13MG-11	-9.377
	11TJ-58-11TJ-62,DL-29-DL-31	-11.347	11TJ-66	-6.227
	13HST-1-13HST-24	-11.291	13NWH-13	-12.071
Liao <i>et al.</i> , 2018	SK14-02-SK14-06	3.650	SK14-02-SK14-06	13.775
	SK15-02-SK15-09	1.088	SK15—01-SK15—09	7.540
Qian <i>et al.</i> , 2017	TS-1-1-TS-4-1	-12.500	TS-1-1-TS-4-10	-11.421
Song <i>et al.</i> , 2018a	ZX14-Zx15-4	-9.387	zx14,zxa33	-8.066
Zhang <i>et al.</i> , 2017c	CJ304-3-4,*06220	-10.325	CJ-1,CJ-2	-10.756
	JF-7,*06173	-10.253	JF-12	-10.211
Huang <i>et al.</i> , 2017	Y05-2-Y06-1,Y11-Y12	-10.868	Y-21	-10.660
	Y03-Y06-2,Ysd-3-1-Ysd-4	-9.568	YSD-1	-9.122
Zhao <i>et al.</i> , 2016b	06MES-10A- 06MES-14C	-9.071	06MES-10A, 06MES-14A	-6.065
	06SZJ-06, 06DZS-02	-10.850	06SZJ-06B	-6.232
	06DZS-01A- 06DZS-10B	-10.500	DZS-01A	-9.700
Zhao <i>et al.</i> , 2017b	B1307-1-B1405-1	-4.300	B1310-1,B1403-1	2.400
Fu <i>et al.</i> , 2015	X01-1-X01-7	-4.607	ZJ18-3	-4.055
Xia <i>et al.</i> , 2014	XW01-XW07	-4.300	XW01	1.644
	DT01-DT09	-0.800	DT01-DT09	5.172
Wang <i>et al.</i> , 2015b	10ZYS-05	-12.500	10ZYS05	-8.736
Gao <i>et al.</i> , 2014a	10SC09-10SC55	-10.317	10SC55A	-10.156
	10SC05 -10SC63	-10.633	10SC51	-9.617
	10SC15-10SC17,FCH1-FCH12	-10.183	10SC17	-8.225



Sample	Er	Tm	Yb	Lu	W	Tl	Pb	Bi	Th	U	Ta	Hf
GBPG-1	1.85	0.31	1.92	0.32	0.31	0.30	14.60	0.04	11.9	0.90	0.40	5.9
GBPG-1	1.81	0.30	1.88	0.34	0.33	0.38	14.90	0.06	11.1	0.90	3.83	5.2
GBPG-1	1.88	0.32	1.98	0.32	0.35	0.39	14.00	0.10	11.4	0.90	4.00	6.4
GBPG-1	1.86	0.32	2.09	0.34	0.27	0.30	14.20	0.04	11.1	0.90	4.20	5.0
GBPG-1	1.85	0.27	2.20	0.33	0.29	0.40	13.70	0.07	10.8	0.80	3.90	6.0
GSR-1	6.50	1.06	7.40	1.15	8.40	1.93	31.00	0.60	54.0	19.00	7.20	5.9
GSR-1	6.10	1.03	7.57	1.18	8.66	1.96	29.17	0.59	55.8	18.41	7.21	5.7
GSR-1	6.90	1.02	6.99	1.16	8.37	1.98	29.78	0.58	52.5	19.88	7.06	6.0
GSR-1	6.20	1.03	7.59	1.07	8.69	1.91	29.08	0.60	55.6	19.24	7.28	5.5
GSR-1	6.50	1.09	7.00	1.13	8.68	1.96	32.43	0.62	53.4	19.36	7.23	5.8

Table S-5-3 Whole rock Nd isotopic compositions for standard materials during analysis

Sample	$^{143}\text{Nd}/^{144}\text{Nd}$	2σ
BCR-1	0.512661	6
BCR-1	0.512663	8
BCR-1	0.512663	8
BCR-1	0.512661	6
BCR-1	0.512662	4
La Jolla	0.511861	6
La Jolla	0.511862	6
La Jolla	0.511863	8
La Jolla	0.511862	6
La Jolla	0.511864	8

Table S-5-4 Whole rock Hf isotopic compositions for standard materials during analysis.

Sample	$^{176}\text{Hf}/^{177}\text{Hf}$	2σ	$^{178}\text{Hf}/^{177}\text{Hf}$	2σ
AGV-2	0.282976	0.000002	1.46718	0.00001
AGV-2	0.282990	0.000002	1.46725	0.00000
AGV-2	0.282985	0.000003	1.46722	0.00001
AGV-2	0.282986	0.000003	1.46723	0.00001
AGV-2	0.282985	0.000003	1.46722	0.00001
BCR-2	0.282874	0.000002	1.46727	0.00001
BCR-2	0.282871	0.000002	1.46719	0.00001
BCR-2	0.282868	0.000002	1.46725	0.00000
BCR-2	0.282885	0.000002	1.46720	0.00001
BCR-2	0.282864	0.000004	1.46720	0.00001
BHVO-2	0.283102	0.000001	1.46726	0.00001
BHVO-2	0.283096	0.000002	1.46718	0.00001
BHVO-2	0.283090	0.000003	1.46718	0.00001
BHVO-2	0.283093	0.000003	1.46723	0.00001
BHVO-2	0.283093	0.000003	1.46723	0.00001
RGM-2	0.283021	0.000004	1.46720	0.00001
RGM-2	0.283022	0.000004	1.46720	0.00001
RGM-2	0.283020	0.000003	1.46721	0.00001
RGM-2	0.283019	0.000003	1.46721	0.00001
RGM-2	0.283021	0.000004	1.46720	0.00001



Table S-5-5 Zircon Hf isotopic compositions for standard materials during analysis

sample	$^{176}\text{Hf}/^{177}\text{Hf}$	2σ	$^{176}\text{Yb}/^{177}\text{Hf}$	2σ	$^{176}\text{Lu}/^{177}\text{Hf}$	2σ
91500	0.282311	0.000047	0.007184	0.000072	0.000276	0.000001
91500	0.282314	0.000038	0.007089	0.000082	0.000275	0.000001
91500	0.282291	0.000035	0.007341	0.000086	0.000277	0.000001
91500	0.282305	0.000031	0.009413	0.000032	0.000278	0.000000
91500	0.282233	0.000045	0.012642	0.000028	0.000329	0.000000
91500	0.282315	0.000055	0.012684	0.000071	0.000323	0.000000
91500	0.282312	0.000054	0.012487	0.000023	0.000321	0.000000
91500	0.282324	0.000047	0.007172	0.000034	0.000275	0.000001
91500	0.282303	0.000032	0.007185	0.000047	0.000274	0.000001
91500	0.282282	0.000043	0.007202	0.000075	0.000284	0.000001
91500	0.282304	0.000017	0.011595	0.000054	0.000307	0.000001
91500	0.282294	0.000015	0.011217	0.000065	0.000305	0.000001
91500	0.282305	0.000014	0.010637	0.000065	0.000297	0.000001
91500	0.282305	0.000027	0.010437	0.000042	0.000295	0.000000
91500	0.282323	0.000016	0.009545	0.000028	0.000287	0.000000
91500	0.282304	0.000077	0.010275	0.000084	0.000307	0.000000
Mud Tank	0.282484	0.000027	0.001835	0.000033	0.000055	0.000001
Mud Tank	0.282484	0.000047	0.001892	0.000021	0.000054	0.000001
Mud Tank	0.282487	0.000025	0.001912	0.000017	0.000054	0.000001
Mud Tank	0.282483	0.000035	0.001957	0.000036	0.000061	0.000000
Mud Tank	0.282484	0.000033	0.001811	0.000022	0.000051	0.000001
Mud Tank	0.282488	0.000041	0.001963	0.000031	0.000059	0.000000
Mud Tank	0.282475	0.000032	0.001877	0.000024	0.000052	0.000000
Mud Tank	0.282471	0.000041	0.001899	0.000019	0.00006	0.000001
Mud Tank	0.282399	0.000043	0.001921	0.000018	0.000065	0.000001
Mud Tank	0.282455	0.000037	0.001898	0.000036	0.000058	0.000001
Mud Tank	0.282487	0.000035	0.001985	0.000033	0.000057	0.000000
Mud Tank	0.282432	0.000036	0.001899	0.000036	0.000051	0.000001
Mud Tank	0.282387	0.000031	0.00185	0.000039	0.000062	0.000001
Mud Tank	0.282481	0.000052	0.001882	0.000025	0.000064	0.000000
Mud Tank	0.282483	0.000021	0.00185	0.000021	0.000058	0.000000
Mud Tank	0.282483	0.000023	0.001943	0.000038	0.000059	0.000001



Table S-5-6 Zircon O isotopic compositions for standard materials during analysis.

Sample	$^{18}\text{O}/^{16}\text{O}$	1 s.e.	$^{18}\text{O}_\text{R}$	$^{18}\text{O}_\text{C}$	2 s.e.
91500	0.002017071	0.008729563	10.20	5.97	0.19
91500	0.002017054	0.007740212	10.10	5.89	0.18
91500	0.002017191	0.012069925	10.20	5.98	0.20
91500	0.002017183	0.011332486	10.16	5.95	0.23
91500	0.002017192	0.010963056	10.16	5.96	0.21
91500	0.002017014	0.010450853	10.17	5.96	0.16
91500	0.002017164	0.009839817	10.08	5.91	0.21
91500	0.002017051	0.011551639	10.07	5.90	0.19
91500	0.002017004	0.012035082	10.13	5.94	0.16
91500	0.002017004	0.007740562	10.20	5.98	0.22
91500	0.002017191	0.013136341	10.20	5.98	0.24
PENGLAI	0.002018838	0.009548955	6.8	5.33	0.21
PENGLAI	0.002018794	0.012893091	6.78	5.31	0.29
PENGLAI	0.002018874	0.007266366	6.82	5.35	0.16
PENGLAI	0.002019644	0.012199558	7.2	5.7	0.21
PENGLAI	0.002018236	0.010900021	6.5	5.03	0.23
PENGLAI	0.002018267	0.011877535	6.52	5.05	0.26
PENGLAI	0.002018559	0.010167726	6.66	5.16	0.22
PENGLAI	0.002018433	0.007492875	6.6	5.13	0.13
PENGLAI	0.002018661	0.008254897	6.71	5.24	0.17
PENGLAI	0.002019292	0.012255554	7.03	5.56	0.26
PENGLAI	0.002019344	0.009568334	7.05	5.55	0.18



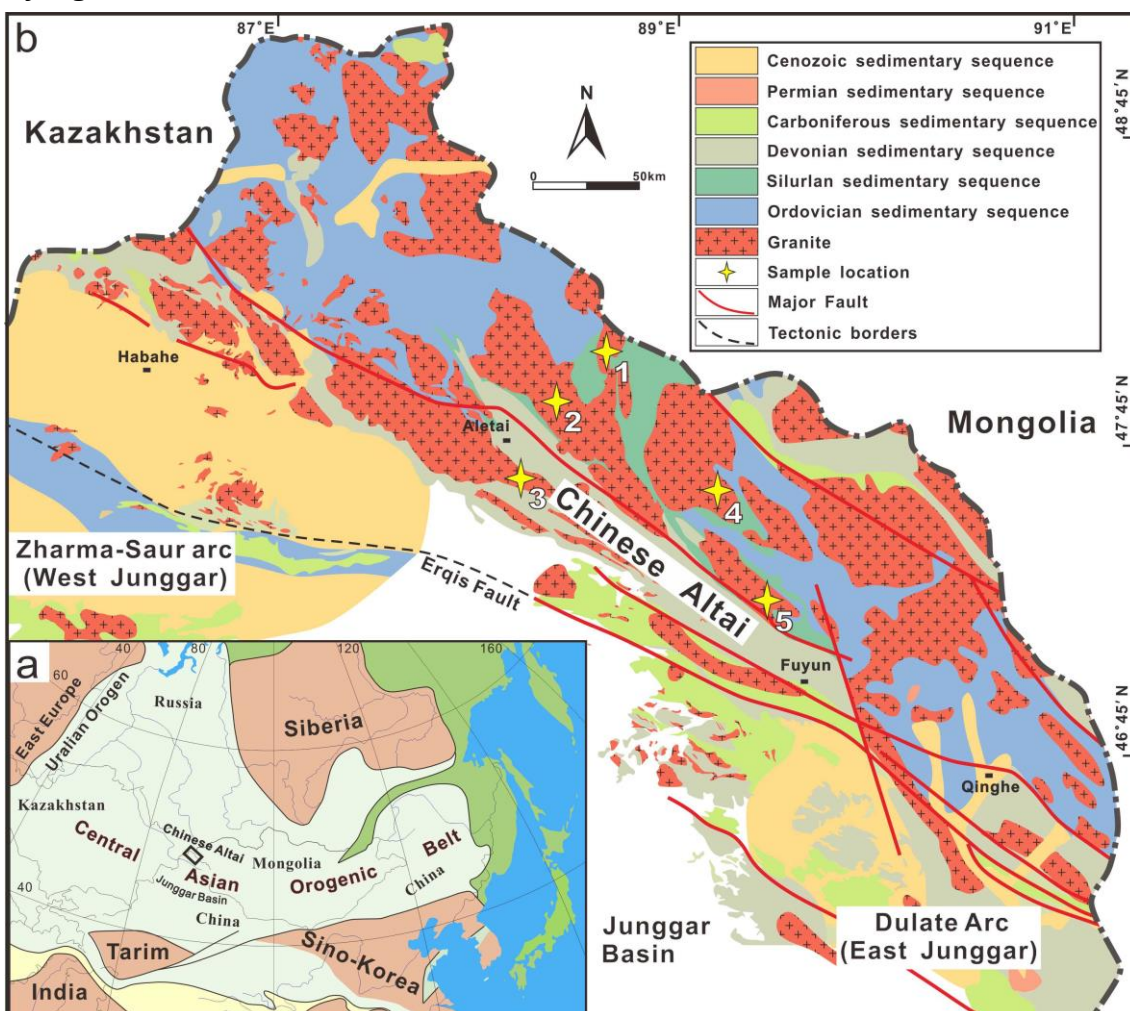
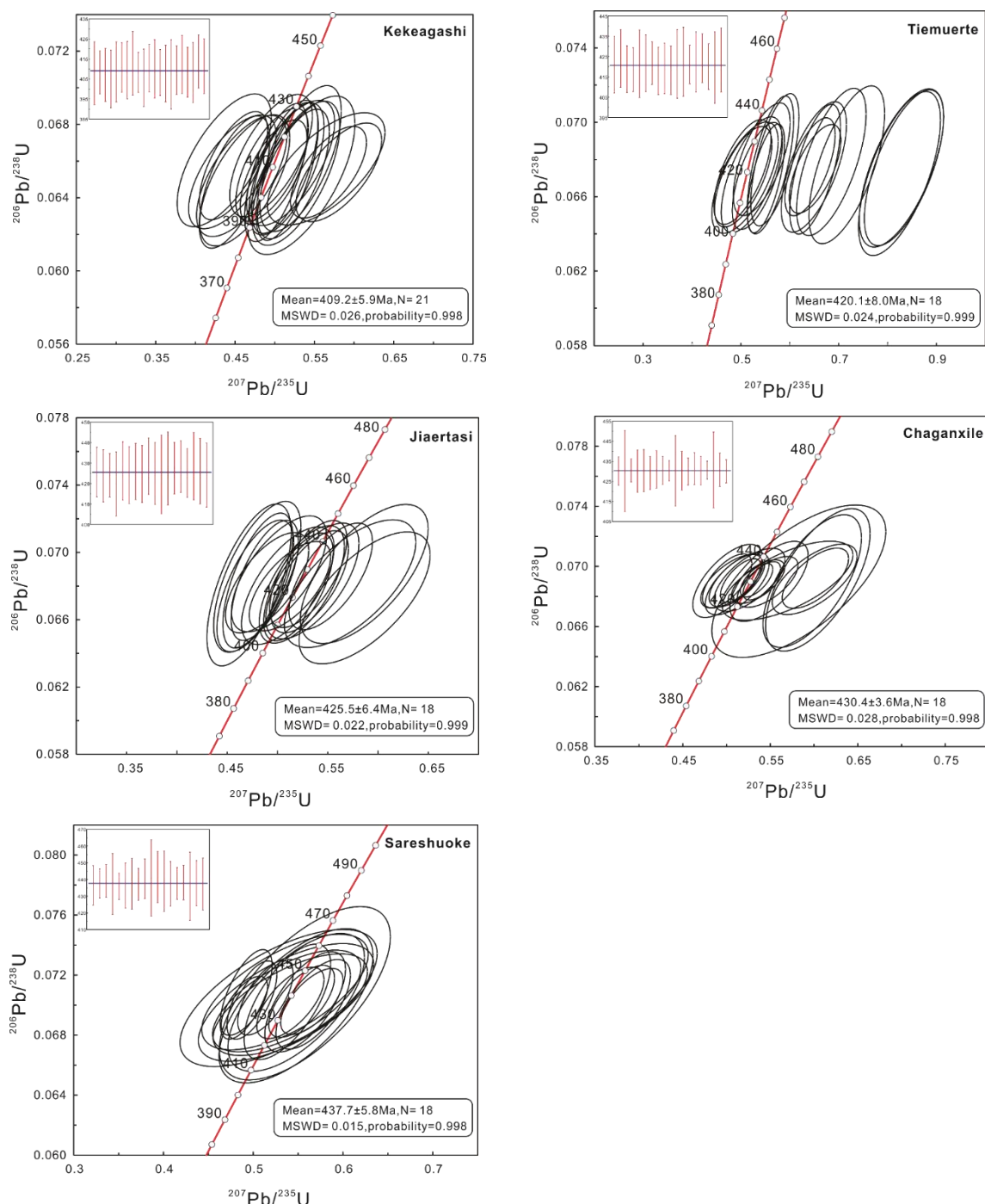
Supplementary Figures

Figure S-1 (a) Location of northern Xinjiang in the Central Asian Orogenic Belt (modified after Zhang *et al.*, 2019); (b) Geological map showing the distribution of the studied granites in the Chinese Altai (modified after Zhang *et al.*, 2019), including: 1. the Kekeagashi pluton, 2. the Tiemuerte pluton, 3. the Jiaertasi pluton, 4. the Chaganxile pluton, and 5. the Sareshuoke pluton.



**Figure S-2** U - Pb concordia diagrams of the studied granites.

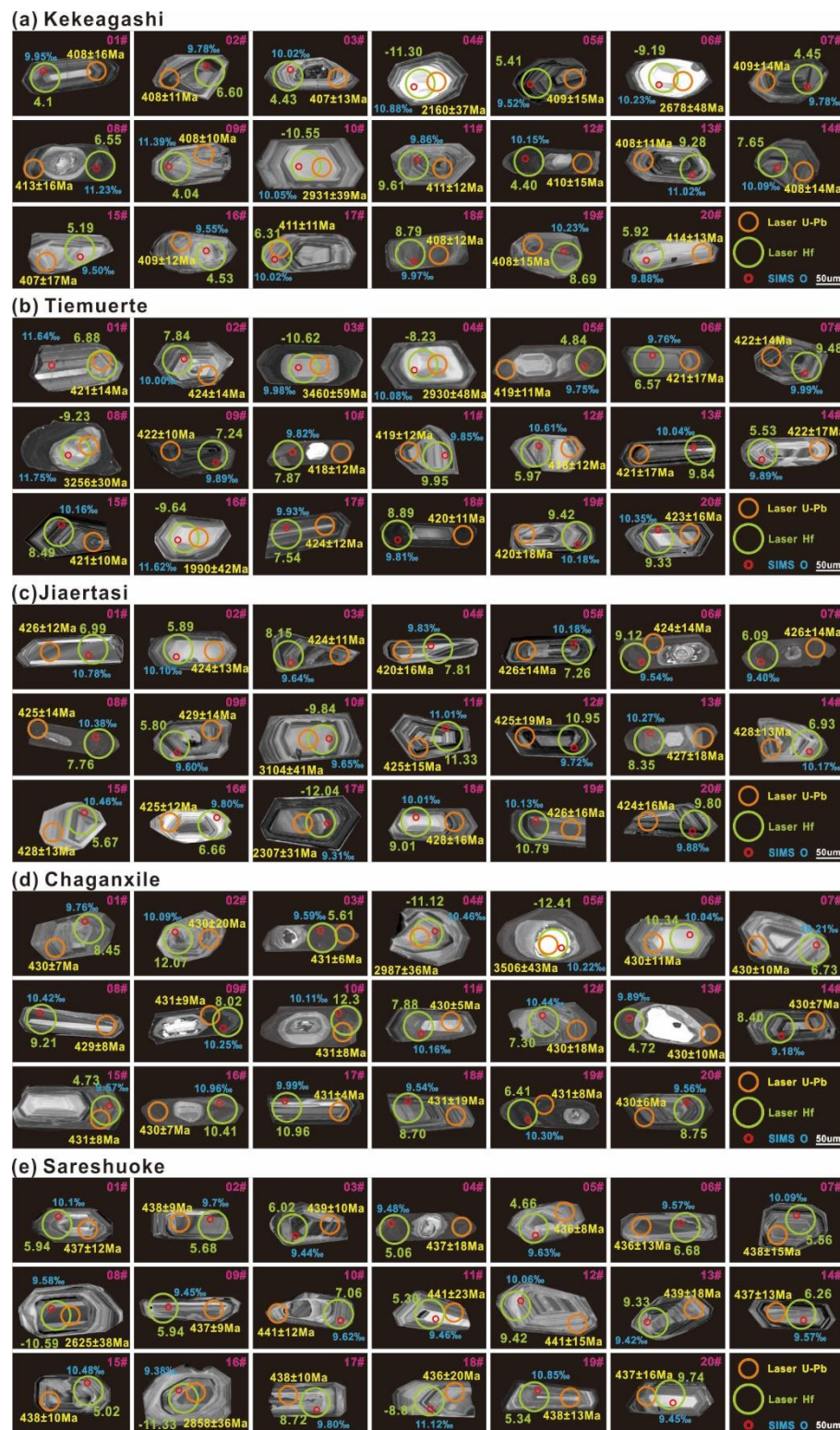


Figure S-3 CL images of zircon grains from the studied granites with analytical spots for age values, $\epsilon_{\text{Hf}}(t)$ values and $\delta^{18}\text{O}$ compositions.



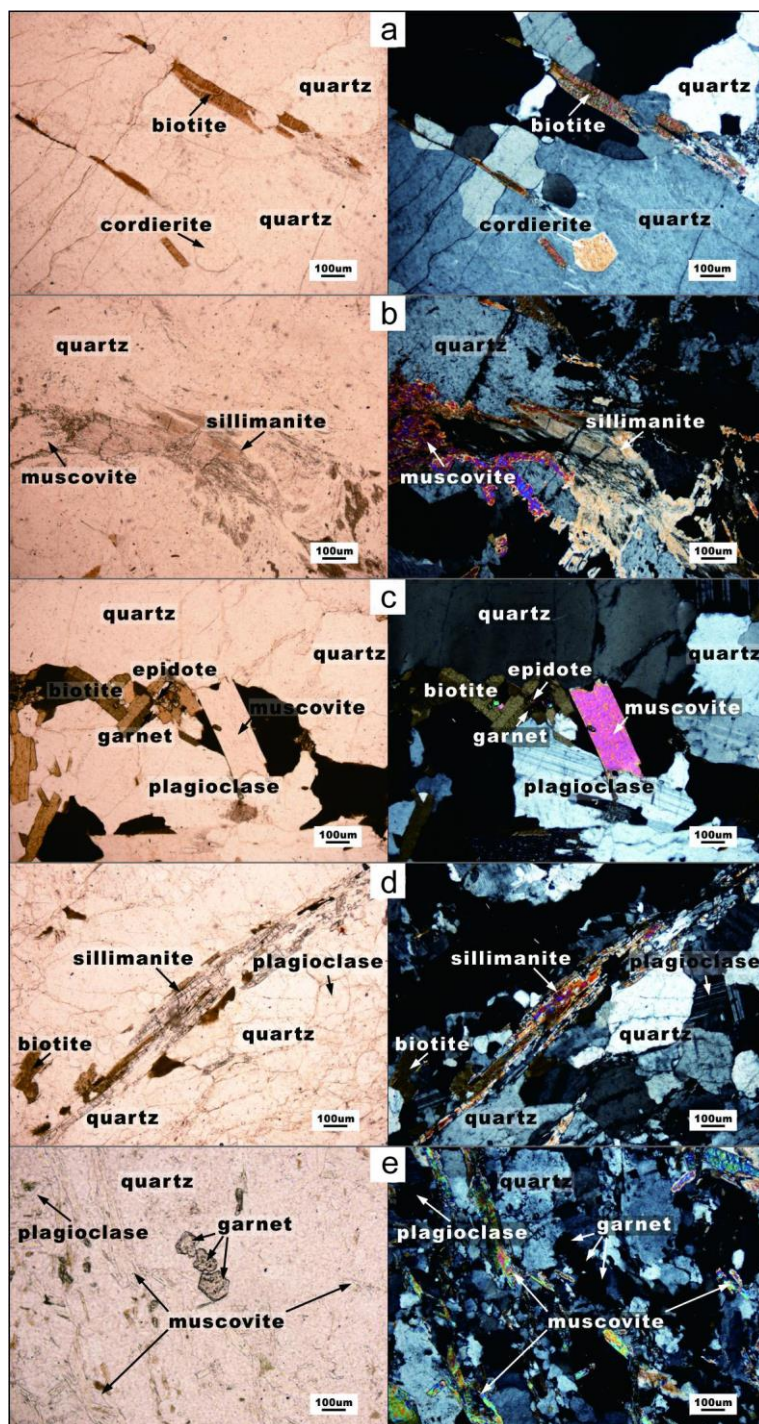


Figure S-4 Photomicrographs from the studied granites of the (a) Kekeagashi, (b) Tiemuerte, (c) Jiaertasi, (d) Chaganxile, and (e) Sareshuoke plutons.



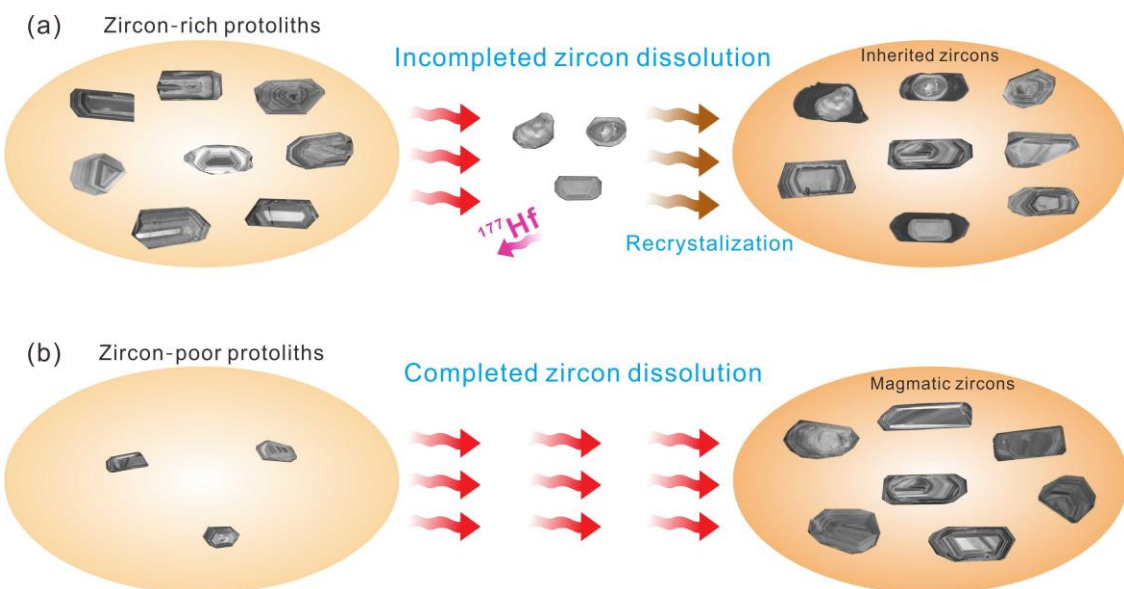


Figure S-5 Schematic diagram suggesting the different melting processes of (a) zircon-rich and (b) zircon-poor protoliths.

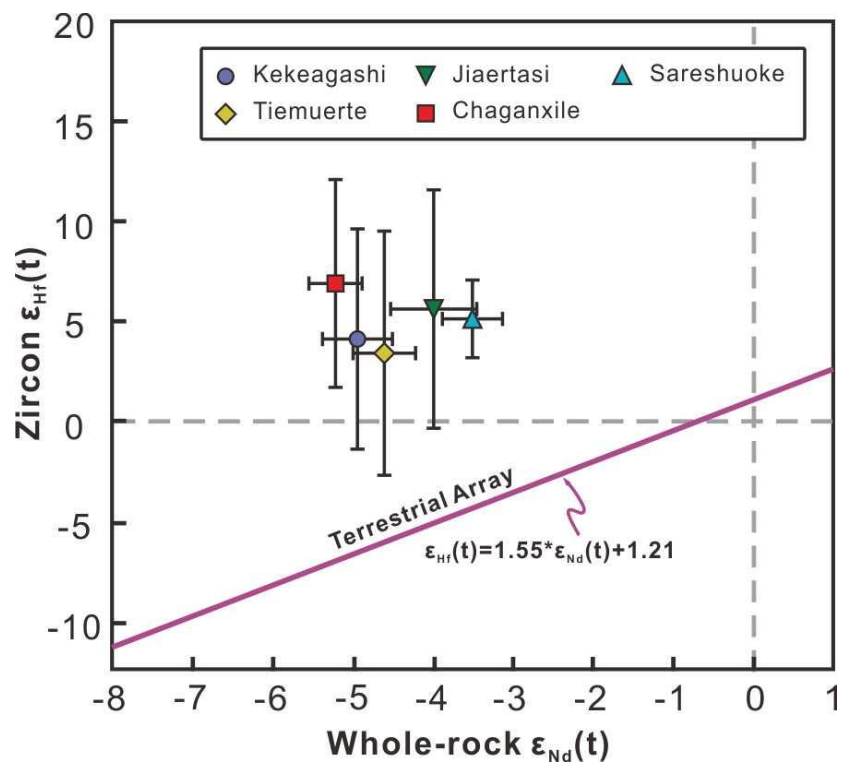


Figure S-6 Crossplot of zircon $\epsilon_{\text{Hf}}(t)$ versus whole-rock $\epsilon_{\text{Nd}}(t)$.



Supplementary Information References

- Bao, Z., Cai, K., Sun, M., Xiao, W., Wan, B., Wang, Y., Xia, X. (2018) Continental crust melting induced by subduction initiation of the South Tianshan Ocean: Insight from the Latest Devonian granitic magmatism in the southern Yili Block, NW China. *Journal of Asian Earth Sciences* 153, 100-117.
- Cai, D.W., Tang, Y., Zhang, H., Lv, Z.H., Liu, Y.L. (2017) Petrogenesis and tectonic setting of the Devonian Xiqin A-type granite in the northeastern Cathaysia Block, SE China. *Journal of Asian Earth Sciences* 141, Part A, 43-58.
- Cao, M., Qin, K., Li, G., Evans, N.J., Hollings, Jin, L. (2016) Genesis of ilmenite-series I-type granitoids at the Baogutu reduced porphyry Cu deposit, western Junggar, NW-China. *Lithos* 246–247, 13-30.
- Cao, M., Qin, K., Li, G., Evans, N.J., McLennan, B.I., Lu, W., Deng, G. (2017) Petrogenesis of the Baishan granite stock, Eastern Tianshan, NW China. Geodynamic setting and implications for potential mineralization. *Lithos* 292–293, 278-293.
- Cao, X., Lü, X., Yuan, Q., Wang, X., Liu, H., Shen, W. (2014) Neoproterozoic granitic activities in the Xingdi plutons at the Kuluketage block, NW China. Evidence from zircon U-Pb dating, geochemical and Sr-Nd-Hf isotopic analyses. *Journal of Asian Earth Sciences* 96, 93-107.
- Chen, B., Long, X., Wilde, S.A., Yuan, C., Wang, Q., Xia, X., Zhang, Z. (2017a) Delamination of lithospheric mantle evidenced by Cenozoic potassic rocks in Yunnan, SW China: A contribution to uplift of the Eastern Tibetan Plateau. *Lithos* 284, 709-729.
- Chen, J.Y., Yang, J.H., Zhang, J.H., & Sun, J.F. (2014) Geochemical transition shown by Cretaceous granitoids in southeastern China. Implications for continental crustal reworking and growth. *Lithos* 196–197, 115-130.
- Chen, J.Y., Yang, J.H., Zhang, J.H., Sun, J.F., Wilde, S.A. (2013a) Petrogenesis of the Cretaceous Zhangzhou batholith in southeastern China. Zircon U-Pb age and Sr-Nd-Hf-O isotopic evidence. *Lithos* 162–163, 140-156.
- Chen, K., Gao, S., Wu, Y., Guo, J., Hu, Z., Liu, Y., Zong, K.Q., Liang, Z.W., Geng, X. (2013b) 2.6–2.7Ga crustal growth in Yangtze craton, South China. *Precambrian Research* 224, 472-490.
- Chen, M., Sun, M., Buslov, M. M., Cai, K., Zhao, G., Kulikova, A. V., Rubanova, E. S. (2016a) Crustal melting and magma mixing in a continental arc setting: Evidence from the Yaloman intrusive complex in the Gorny Altai terrane, Central Asian Orogenic Belt. *Lithos* 252, 76-91.
- Chen, Q., Sun, M., Zhao, G., Yang, F., Long, X., Li, J., Yu, Y. (2017b) Origin of the mafic microgranular enclaves (MMEs) and their host granitoids from the Tagong pluton in Songpan-Ganze terrane: An igneous response to the closure of the Paleo-Tethys ocean. *Lithos* 290, 1-17.
- Chen, W., Xu, Z., Qiu, W., Li, C., Yu, Y., Wang, H., Su, Y. (2015a) Petrogenesis of the Yaochong granite and Mo deposit, Western Dabie orogen, eastern-central China: Constraints from zircon U-Pb and molybdenite Re-Os ages, whole-rock geochemistry and Sr-Nd-Pb-Hf isotopes. *Journal of Asian Earth Sciences* 103, 198-211.
- Chen, X.C., Hu, R.Z., Bi, X.W., Zhong, H., Lan, J.B., Zhao, C.H., Zhu, J.J. (2015b) Petrogenesis of metaluminous A-type granitoids in the Tengchong-Lianghe tin belt of southwestern China. Evidences from zircon U-Pb ages and Hf-O isotopes, and whole-rock Sr-Nd isotopes. *Lithos* 212–215, 93-110.
- Chen, X.C., Hu, R.Z., Bi, X.W., Zhong, H., Lan, J.B., Zhao, C.H., Zhu, J.J. (2015c) Zircon U-Pb ages and Hf-O isotopes, and whole-rock Sr-Nd isotopes of the Bozhushan granite, Yunnan province, SW China. Constraints on petrogenesis and tectonic setting. *Journal of Asian Earth Sciences* 99, 57-71.
- Chen, Z.H., Xing, G.F. (2016b) Geochemical and zircon U-Pb-Hf-O isotopic evidence for a coherent Paleoproterozoic basement beneath the Yangtze Block, South China. *Precambrian Research* 279, 81-90.
- Cheng, Z., Zhang, Z., Santosh, M., Zhao, Z., Chen, L. (2017) Late Carboniferous to early Permian partial melting of the metasedimentary rocks and crustal reworking in the Central Asian Orogenic Belt: Evidence from garnet-bearing rhyolites in the Chinese South Tianshan. *Lithos* 282, 373-387.
- Dan, W., Li, X. H., Wang, Q., Wang, X. C., Wyman, D. A., Liu, Y. (2016) Phanerozoic amalgamation of the Alxa Block and North China Craton: Evidence from Paleozoic granitoids, U-Pb geochronology and Sr-Nd-Pb-Hf-O isotope geochemistry. *Gondwana Research* 32, 105-121.
- Dan, W., Li, X.H., Wang, Q., Wang, X.C., Liu, Y., Wyman, D.A. (2014) Paleoproterozoic S-type granites in the Helanshan Complex, Khondalite Belt, North China Craton: Implications for rapid sediment recycling during slab break-off. *Precambrian Research* 254, 59-72.
- Deng, K., Li, Q., Chen, Y., Zhang, C., Zhu, X., Xu, Q. (2018) Geochronology, geochemistry and Sr-Nd-Pb-Hf isotopes of the Early Jurassic granodiorite from the Sankuanggou intrusion, Heilongjiang Province, Northeastern China. Petrogenesis and geodynamic implications. *Lithos* 296–299, 113-128.
- Deng, X., Peng, T., Zhao, T. (2016) Geochronology and geochemistry of the late Paleoproterozoic aluminous A-type granite in the Xiaoqinling area along the southern margin of the North China Craton. Petrogenesis and tectonic implications. *Precambrian Research* 285, 127-146.
- Ding, Q.F., Jiang, S.Y., Sun, F.Y. (2014) Zircon U-Pb geochronology, geochemical and Sr-Nd-Hf isotopic compositions of the Triassic granite and diorite dikes from the Wulonggou mining area in the Eastern Kunlun Orogen, NW China. Petrogenesis and tectonic implications. *Lithos* 205, 266-283.
- Dong, G., Luo, M., Mo, X., Zhao, Z., Dong, L., Yu, X., Liu, Y. (2018) Petrogenesis and tectonic implications of early Paleozoic granitoids in East Kunlun Belt: evidences from geochronology, geochemistry and isotopes. *Geoscience Frontiers* 9, 1383-1397.
- Feng, C., Wang, H., Xiang, X., Zhang, M. (2018) Late Mesozoic granite-related W-Sn mineralization in the northern Jiangxi region, SE China: A review. *Journal of Geochemical Exploration* 195, 31-48.
- Feng, S.J., Zhao, K.D., Ling, H.F., Chen, R., Chen, W.F., Sun, T., Jiang, S.Y., Pu, W. (2014) Geochronology, elemental and Nd-Hf isotopic geochemistry of Devonian A-type granites in central Jiangxi, South China. Constraints on petrogenesis and post-collisional extension of the Wuyi-Yunkai orogeny. *Lithos* 206–207, 1-18.
- Fu, J., Liang, X., Zhou, Y., Wang, C., Jiang, Y., Zhong, Y. (2015) Geochemistry, zircon U-Pb geochronology and Hf isotopes of granitic rocks in the Xiteshan area, North Qaidam, Northwest China: Implications for Neoproterozoic geodynamic evolutions of North Qaidam. *Precambrian Research* 264, 11-29.
- Gao, P., Zhao, Z.F., Zheng, Y.F. (2014a) Petrogenesis of Triassic granites from the Nanling Range in South China: implications for geochemical diversity in granites. *Lithos* 210, 40-56.
- Gao, X. Y., Zhao, T. P., Bao, Z. W., Yang, A. Y. (2014b) Petrogenesis of the early Cretaceous intermediate and felsic intrusions at the southern margin of the North China Craton. Implications for crust-mantle interaction. *Lithos* 206–207, 65-78.
- Gao, X. Y., Zhao, T. P., Chen, W. T. (2014c) Petrogenesis of the early Cretaceous Funiushan granites on the southern margin of the North China Craton: Implications for the Mesozoic geological evolution. *Journal of Asian Earth Sciences* 94, 28-44.
- Gao, X., Yang, L.Q., Meng, J.Y., Zhang, L.J. (2017) Zircon U-Pb, molybdenite Re-Os geochronology and Sr-Nd-Pb-Hf-O-S isotopic constraints on the genesis of Relin Cu-Mo deposit in Zhongdian, Northwest Yunnan, China. *Ore Geology Reviews* 91, 945-962.
- Gao, Y., Mao, J.W., Ye, H.S., Li, Y.F., Luo, Z. Z., Yang, Z.Q. (2016) Petrogenesis of ore-bearing porphyry from the Tangjiaping porphyry Mo deposit, Dabie orogen. Zircon U-Pb geochronology, geochemistry and Sr-Nd-Hf isotopic constraints. *Ore Geology Reviews* 79, 288-300.
- Gou, L.L., Zhang, L.F., Lü, Z., Shen, T.T. (2015) Geochemistry and geochronology of S-type granites and their coeval MP/HT meta-sedimentary rocks in Chinese Southwest Tianshan and their tectonic implications. *Journal of Asian Earth Sciences* 107, 151-171.



- Gu, H., Yang, X., Deng, J., Duan, L., Liu, L. (2017) Geochemical and zircon U-Pb geochronological study of the Yangshan A-type granite. Insights into the geological evolution in south Anhui, eastern Jiangnan Orogen. *Lithos* 284–285, 156–170.
- Guo, C., Chen, Y., Zeng, Z., Lou, F. (2012) Petrogenesis of the Xihuashan granites in southeastern China. Constraints from geochemistry and in-situ analyses of zircon U-Pb-Hf-O isotopes. *Lithos* 148, 209–227.
- Guo, N.X., Zhao, Z., Gao, J.F., Chen, W., Wang, D.H., Chen, Y.C. (2018) Magmatic evolution and W-Sn-U-Nb-Ta mineralization of the Mesozoic Jiulongnao granitic complex, Nanling Range, South China. *Ore Geology Reviews* 94, 414–434.
- Gürsu, S., Mueller, A., Sunkari, E.D., Möller, A., Köksal, S., Kamenov, G.D., Göncüoğlu, M.C. (2018) Nd, Pb, Hf isotope characteristics and provenance of glacial granitic pebbles from Late Ordovician diamictites in the Taurides, S Turkey. *Gondwana Research* 54, 205–216.
- He, D. F., Zhu, W. G., Zhong, H., Ren, T., Bai, Z. J., Fan, H. P. (2013) Zircon U-Pb geochronology and elemental and Sr–Nd–Hf isotopic geochemistry of the Daocheng granitic pluton from the Yidun Arc, SW China. *Journal of Asian Earth Sciences* 67, 1–17.
- He, W., Xie, S., Liu, X., Gao, X., Xing, Y. (2018a) Geochronology and geochemistry of the Donglufang porphyry-skarn Mo–Cu deposit in the southern Yidun Terrane and their geological significances. *Geoscience Frontiers* 9, 1433–1450.
- He, W., Yang, L., Lu, Y., Jeon, H., Xie, S., Gao, X. (2018b) Zircon U-Pb dating, geochemistry and Sr–Nd–Hf–O isotopes for the Baimaxueshan granodiorites and mafic microgranular enclaves in the Sanjiang Orogen. Evidence for westward subduction of Paleo-Tethys. *Gondwana Research* 62, 112–126.
- Hu, P.Y., Zhai, Q.G., Jahn, B.M., Wang, J., Li, C., Lee, H.Y., Tang, S.H. (2015) Early Ordovician granites from the South Qiangtang terrane, northern Tibet: Implications for the early Paleozoic tectonic evolution along the Gondwanan proto-Tethyan margin. *Lithos* 220, 318–338.
- Hu, Q., Yu, K., Liu, Y., Hu, Z., Zong, K. (2017) The 131–134 Ma A-type granites from northern Zhejiang Province, South China. Implications for partial melting of the Neoproterozoic lower crust. *Lithos* 294–295, 39–52.
- Hu, Y., Niu, Y., Li, J., Ye, L., Kong, J., Chen, S., Zhang, Y., Zhang, G. (2016) Petrogenesis and tectonic significance of the late Triassic mafic dikes and felsic volcanic rocks in the East Kunlun Orogenic Belt, Northern Tibet Plateau. *Lithos* 245, 205–222.
- Huang, H., Niu, Y., Nowell, G., Zhao, Z., Yu, X., Mo, X. (2015) The nature and history of the Qilian Block in the context of the development of the Greater Tibetan Plateau. *Gondwana Research* 28, 209–224.
- Huang, L.C., Jiang, S.Y. (2014) Highly fractionated S-type granites from the giant Dahutang tungsten deposit in Jiangnan Orogen, Southeast China: geochronology, petrogenesis and their relationship with W-mineralization. *Lithos* 202, 207–226.
- Huang, W., Wu, J., Zhang, J., Liang, H.Y., Qiu, X.L. (2017) Geochemistry and Hf–Nd isotope characteristics and forming processes of the Yuntoujie granites associated with W–Mo deposit, Guangxi, South China. *Ore Geology Reviews* 81, 953–964.
- Jia, L., Mao, J., Liu, Li, Y. (2018) Petrogenesis of the late Early Cretaceous granodiorite – Quartz diorite from eastern Guangdong, SE China. Implications for tectono-magmatic evolution and porphyry Cu–Au–Mo mineralization. *Lithos* 304–307, 388–411.
- Jiang, H., Jiang, S.Y., Li, W.Q., Zhao, K.D., Peng, N.J. (2018a) Highly fractionated Jurassic I-type granites and related tungsten mineralization in the Shirenzhang deposit, northern Guangdong, South China. Evidence from cassiterite and zircon U–Pb ages, geochemistry and Sr–Nd–Pb–Hf isotopes. *Lithos* 312–313, 186–203.
- Jiang, H., Li, W.Q., Jiang, S.Y., Wang, H., Wei, X. (2017) Geochronological, geochemical and Sr–Nd–Hf isotopic constraints on the petrogenesis of Late Cretaceous A-type granites from the Sibumasu Block, Southern Myanmar, SE Asia. *Lithos* 268–271, 32–47.
- Jiang, X.Y., Luo, J.C., Guo, J., Wu, K., Zhang, Z.K., Sun, W.D., Xia, X. (2018b) Geochemistry of I- and A-type granites of the Qingyang–Jiuhuashan complex, eastern China. Insights into early cretaceous multistage magmatism. *Lithos* 316–317, 278–294.
- Jiang, Y.H., Zhou, Q., Liao, S.Y., Jin, G.D. (2011) Petrogenesis and tectonic implications of Early Cretaceous S- and A-type granites in the northwest of the Gan-Hang rift, SE China. *Lithos* 121, 55–73.
- Jones, G.U., Smith, L.B. (1995) The Chemistry of Hydrogen. In: James, B.S., Berlin, R.N. (Eds.) *The Elements from A to Z*. Smith-Publishing Inc., New York, 21–34.
- Karsli, O., Dokuz, A., Kandemir, R. (2016) Subduction-related Late Carboniferous to Early Permian Magmatism in the Eastern Pontides, the Camlik and Casurluk plutons: Insights from geochemistry, whole-rock Sr–Nd and in situ zircon Lu–Hf isotopes, and U–Pb geochronology. *Lithos* 266, 98–114.
- Kita, N.T., Ushikubo, T., Fu, B., Valley, J.W. (2009) High precision SIMS oxygen isotope analysis and the effect of sample topography. *Chemical Geology* 264, 43–57.
- Konopelko, D., Wilde, S.A., Seltmann, R., Romer, R.L., Biske, Y.S. (2018) Early Permian intrusions of the Alai range. Understanding tectonic settings of Hercynian post-collisional magmatism in the South Tien Shan, Kyrgyzstan. *Lithos* 302–303, 405–420.
- Lan, T.G., Fan, H.R., Yang, K.F., Cai, Y.C., Wen, B.J., Zhang, W. (2015) Geochronology, mineralogy and geochemistry of alkali-feldspar granite and albite granite association from the Changyi area of Jiao-Liao-Ji Belt. Implications for Paleoproterozoic rifting of eastern North China Craton. *Precambrian Research* 266, 86–107.
- Li, D., He, D., Santosh, M., Ma, D. (2015a) Tectonic framework of the northern Junggar Basin Part II: The island arc basin system of the western Luliang Uplift and its link with the West Junggar terrane. *Gondwana Research* 27, 1110–1130.
- Li, G., Cao, M., Qin, K., Evans, N.J., Hollings, Seitmuratova, E.Y. (2016a) Geochronology, petrogenesis and tectonic settings of pre- and syn-ore granites from the W–Mo deposits (East Kounrad, Zhanet and Akshatau), Central Kazakhstan. *Lithos* 252–253, 16–31.
- Li, G.M., Li, J.X., Zhao, J.X., Qin, K.Z., Cao, M.J., Evans, N.J. (2015b) Petrogenesis and tectonic setting of Triassic granitoids in the Qiangtang terrane, central Tibet: Evidence from U–Pb ages, petrochemistry and Sr–Nd–Hf isotopes. *Journal of Asian Earth Sciences* 105, 443–455.
- Li, H., Palinkaš, L.A., Watanabe, K., Xi, X.S. (2018a) Petrogenesis of Jurassic A-type granites associated with Cu–Mo and W–Sn deposits in the central Nanling region, South China. Relation to mantle upwelling and intra-continental extension. *Ore Geology Reviews* 92, 449–462.
- Li, H., Wu, J.H., Evans, N.J., Jiang, W.C., Zhou, Z.K. (2018b) Zircon geochronology and geochemistry of the Xianghualing A-type granitic rocks. Insights into multi-stage Sn–polymetallic mineralization in South China. *Lithos* 312–313, 1–20.
- Li, N.B., Niu, H.C., Shan, Q., Yang, W.B. (2015c) Two episodes of Late Paleozoic A-type magmatism in the Qunjisayi area, western Tianshan. Petrogenesis and tectonic implications. *Journal of Asian Earth Sciences* 113, Part 1, 238–253.
- Li, S., Wilde, S.A., Wang, T. (2013) Early Permian post-collisional high-K granitoids from Liuyuan area in southern Beishan orogen, NW China. Petrogenesis and tectonic implications. *Lithos* 179, 99–119.
- Li, X.H., Li, Z.X., Li, W.X., Liu, Y., Yuan, C., Wei, G., Qi, C. (2007) U–Pb zircon, geochemical and Sr–Nd–Hf isotopic constraints on age and origin of Jurassic I- and A-type granites from central Guangdong, SE China: a major igneous event in response to foundering of a subducted flat-slab? *Lithos* 96(1–2), 186–204.
- Li, X.H., Long, W.G., Li, Q.L., Liu, Y., Zheng, Y.F., Yang, Y.H., Chamberlain, K.R., Wan, D.F., Guo, C.H., Wang, X.C., Tao, H. (2010) Penglai Zircon Megacrysts: A Potential New Working Reference Material for Microbeam Determination of Hf–O Isotopes and U–Pb Age. *Geostandards and Geoanalytical Research* 34, 117–134.
- Li, X.W., Mo, X., Huang, X., Dong, G., Yu, X., Luo, M., Liu, Y. (2015d) U–Pb zircon geochronology, geochemical and Sr–Nd–Hf isotopic compositions of the Early Indosinian Tongren Pluton in West Qinling: Petrogenesis and geodynamic implications. *Journal of Asian Earth Sciences* 97, Part A, 38–50.



- Li, Y.J., Wei, J.H., Santosh, M., Tan, J., Fu, L.B., Zhao, S.Q. (2016b) Geochronology and petrogenesis of Middle Permian S-type granitoid in southeastern Guangxi Province, South China: Implications for closure of the eastern Paleo-Tethys. *Tectonophysics* 682, 1-16.
- Liao, J. P., Jahn, B. M., Alexandrov, I., Chung, S. L., Zhao, P., Ivin, V., Usuki, T. (2018) Petrogenesis of Mid-Eocene granites in South Sakhalin, Russian Far East: Juvenile crustal growth and comparison with granitic magmatism in Hokkaido and Sikhote-Alin. *Journal of Asian Earth Sciences* 167, 103-129.
- Liu, H., Wang, Y., Cawood, P.A., Fan, W., Cai, Y., Xing, X. (2015) Record of Tethyan ocean closure and Indosinian collision along the Ailaoshan suture zone (SW China). *Gondwana Research* 27, 1292-1306.
- Liu, J.F., Li, J.Y., Chi, X.G., Zhao, Z., Hu, Z.C., Feng, Q.W. (2012) Petrogenesis of middle Triassic post-collisional granite from Jiefangyingzi area, southeast Inner Mongolia. Constraint on the Triassic tectonic evolution of the north margin of the Sino-Korean paleoplato. *Journal of Asian Earth Sciences* 60, 147-159.
- Liu, L., Qiu, J. S., Li, Z. (2013) Origin of mafic microgranular enclaves (MMEs) and their host quartz monzonites from the Muchen pluton in Zhejiang Province, Southeast China: implications for magma mixing and crust–mantle interaction. *Lithos* 160, 145-163.
- Liu, P., Mao, J., Yao, W., Wang, X., Jia, L., Yang, H. (2017) Petrogenesis of the mafic microgranular enclaves (MMEs) and their host granodiorites from the Zijinshan intrusion along the Middle-Lower Yangtze River Valley: Implications for geodynamic setting and mineralization. *Lithos* 288, 1-19.
- Liu, S., Hu, R., Gao, S., Feng, C., Qi, Y., Wang, T., Feng, G.Y., Coulson, I.M. (2008) U-Pb zircon age, geochemical and Sr-Nd-Pb-Hf isotopic constraints on age and origin of alkaline intrusions and associated mafic dikes from Sulu orogenic belt, Eastern China. *Lithos* 106, 365-379.
- Liu, S., Hu, R., Gao, S., Feng, C., Huang, Z., Lai, S., Wang, T. (2009) U-Pb zircon, geochemical and Sr-Nd-Hf isotopic constraints on the age and origin of Early Palaeozoic I-type granite from the Tengchong-Baoshan Block, Western Yunnan Province, SW China. *Journal of Asian Earth Sciences* 36, 168-182.
- Liu, Z.C., Wu, F.Y., Ji, W.Q., Wang, J.G., Liu, C.Z. (2014) Petrogenesis of the Ramba leucogranite in the Tethyan Himalaya and constraints on the channel flow model. *Lithos* 208, 118-136.
- Luo, B.J., Liu, R., Zhang, H.F., Zhao, J.H., Yang, H., Xu, W.C., Guo, L., Zhang, L.Q., Tao, L., Pan, F.B., Wang, W., Gao, Z., Shao, H. (2018) Neoproterozoic continental back-arc rift development in the Northwestern Yangtze Block: Evidence from the Hannan intrusive magmatism. *Gondwana Research* 59, 27-42.
- Ma, L., Jiang, S. Y., Dai, B. Z., Jiang, Y. H., Hou, M. L., Pu, W., Xu, B. (2013) Multiple sources for the origin of Late Jurassic Linglong adakitic granite in the Shandong Peninsula, eastern China: Zircon U-Pb geochronological, geochemical and Sr-Nd-Hf isotopic evidence. *Lithos* 162, 251-263.
- Ma, L., Wang, Y., Fan, W., Geng, H., Cai, Y., Zhong, H., Xing, X. (2014) Petrogenesis of the early Eocene I-type granites in west Yingjiang (SW Yunnan) and its implication for the eastern extension of the Gangdese batholiths. *Gondwana Research* 25, 401-419.
- Mao, J., Xiong, B., Liu, J., Pirajno, F., Cheng, Y., Ye, H., Dai, P. (2017) Molybdenite Re/Os dating, zircon U-Pb age and geochemistry of granitoids in the Yangchuling porphyry W-Mo deposit (Jiangnan tungsten ore belt), China: Implications for petrogenesis, mineralization and geodynamic setting. *Lithos* 286, 35-52.
- Martínez, E.M., Villaseca, C., Orejana, D., Pérez-Soba, C., Belousova, E., Andersen, T. (2014) Tracing magma sources of three different S-type peraluminous granitoid series by in situ U-Pb geochronology and Hf isotope zircon composition: The Variscan Montes de Toledo batholith (central Spain). *Lithos* 200, 273-298.
- Moghadam, H. S., Li, X. H., Ling, X. X., Santos, J. F., Stern, R. J., Li, Q. L., Ghorbani, G. (2015) Eocene Kashmar granitoids (NE Iran): petrogenetic constraints from U-Pb zircon geochronology and isotope geochemistry. *Lithos* 216, 118-135.
- Nabatian, G., Jiang, S. Y., Honarmand, M., Neubauer, F. (2016) Zircon U-Pb ages, geochemical and Sr-Nd-Pb-Hf isotopic constraints on petrogenesis of the Tarom-Olya pluton, Alborz magmatic belt, NW Iran. *Lithos* 244, 43-58.
- Nance, J.R., Armstrong, J.T., Cody, G.D., Fogel, M.L., Hazen, R.M. (2015) Preserved macroscopic polymeric sheets of shell-binding protein in the Middle Miocene (8 to 18 Ma) gastropod Ecphora. *Geochemical Perspectives Letters* 1, 1-9.
- Niu, X.L., Chen, B., Ma, X. (2011) Petrogenesis of the Dengzhazi A-type pluton from the Taihang-Yanshan Mesozoic orogenic belts, North China Craton. *Journal of Asian Earth Sciences* 41, 133-146.
- Peng, T., Zhao, G., Fan, W., Peng, B., Mao, Y. (2015) Late Triassic granitic magmatism in the Eastern Qiangtang, Eastern Tibetan Plateau: Geochronology, petrogenesis and implications for the tectonic evolution of the Paleo-Tethys. *Gondwana Research* 27, 1494-1508.
- Qian, X., Feng, Q., Wang, Y., Zhao, T., Zi, J. W., Udhachon, M., Wang, Y. (2017) Late Triassic post-collisional granites related to Paleotethyan evolution in SE Thailand: geochronological and geochemical constraints. *Lithos* 286, 440-453.
- Qin, J., Lai, S., Grapes, R., Diwu, C., Ju, Y., Li, Y. (2009) Geochemical evidence for origin of magma mixing for the Triassic monzonitic granite and its enclaves at Mishuling in the Qinling orogen (central China). *Lithos* 112, 259-276.
- Qin, Z.W., Wu, Y.B., Wang, H., Gao, S., Zhu, L.Q., Zhou, L., Yang, S.H. (2014) Geochronology, geochemistry, and isotope compositions of Piaochi S-type granitic intrusion in the Qinling orogen, central China: petrogenesis and tectonic significance. *Lithos* 202, 347-362.
- Qiu, Z., Li, S., Yan, Q., Wang, H., Wei, X., Bu, A. (2017) Late Jurassic Sn metallogeny in eastern Guangdong, SE China coast. Evidence from geochronology, geochemistry and Sr-Nd-Hf-S isotopes of the Dadaoshan Sn deposit. *Ore Geology Reviews* 83, 63-83.
- Shen, X., Zhang, H., Wang, Q., Wyman, D.A., Yang, Y. (2011) Late Devonian-Early Permian A-type granites in the southern Altay Range, Northwest China. Petrogenesis and implications for tectonic setting of "A2-type" granites. *Journal of Asian Earth Sciences* 42, 986-1007.
- Song, S., Mao, J., Zhu, Y., Yao, Z., Chen, G., Rao, J., Ouyang, Y. (2018a) Partial-melting of fertile metasedimentary rocks controlling the ore formation in the Jiangnan porphyry-skarn tungsten belt, south China: A case study at the giant Zhuxi W-Cu skarn deposit. *Lithos* 304, 180-199.
- Song, Z. G., Han, Z. Z., Gao, L. H., Geng, H. Y., Li, X. P., Meng, F. X., Yan, J. L. (2018b) Permo-Triassic evolution of the southern margin of the Central Asian Orogenic Belt revisited: Insights from Late Permian igneous suite in the Daheishan Horst, NE China. *Gondwana Research* 56, 23-50.
- Spencer, C.J., Thomas, R.J., Roberts, N.M., Cawood, P.A., Millar, I., Tapster, S. (2015) Crustal growth during island arc accretion and transcurrent deformation, Natal Metamorphic Province, South Africa: new isotopic constraints. *Precambrian Research* 265, 203-217.
- Su, Y., Zheng, J., Griffin, W. L., Zhao, J., Suzanne, Y. O., Tang, H., Ping, X.Q., Xiong, Q. (2013) Petrogenesis and geochronology of Cretaceous adakitic, I- and A-type granitoids in the NE Yangtze block. Constraints on the eastern subsurface boundary between the North and South China blocks. *Lithos* 175-176, 333-350.
- Sun, L.Q., Ling, H.F., Shen, W.Z., Wang, K.X., Huang, G.L. (2017) Petrogenesis of two Triassic A-type intrusions in the interior of South China and their implications for tectonic transition. *Lithos* 284-285, 642-653.
- Sun, Y., Ma, C., Liu, Y., She, Z. (2011) Geochronological and geochemical constraints on the petrogenesis of late Triassic aluminous A-type granites in southeast China. *Journal of Asian Earth Sciences* 42, 1117-1131.
- Tang, G.J., Wang, Q., Wyman, D.A., Sun, M., Li, Z.X., Zhao, Z.H., Sun, W.D., Jia, X.H., Jiang, Z.Q. (2010) Geochronology and geochemistry of Late Paleozoic magmatic rocks in the Lamasu-Dabate area, northwestern Tianshan (west China). Evidence for a tectonic transition from arc to post-collisional setting. *Lithos* 119, 393-411.
- Tang, G.Q., Li, X.H., Li, Q.L., Liu, Y., Ling, X.X., Yin, Q.Z. (2015) Deciphering the physical mechanism of the topography effect for oxygen isotope measurements using a Cameca IMS-1280 SIMS. *Journal of Analytical Atomic Spectrometry* 30, 950-956.
- Wang, C.C., Liu, Y.C., Zhang, G., Zhao, G.C., Wang, A.D., Song, B. (2017) Zircon U-Pb geochronology and geochemistry of two types of Paleoproterozoic granitoids



- from the southeastern margin of the North China Craton. Constraints on petrogenesis and tectonic significance. *Precambrian Research* 303, 268-290.
- Wang, C.M., Zhang, L., Chen, H., Tang, H., Chen, Y.J., Dong, L.H., Fang, J. (2018) Geochronology, geochemistry and tectonic significance of the ore-associated granites at the Kaladawan Fe–Mo ore field (Altyn), NW China. *Ore Geology Reviews* 100, 457-470.
- Wang, G.G., Ni, P., Yu, W., Chen, H., Jiang, L.L., Wang, B.H., Li, P.F. (2014a) Petrogenesis of Early Cretaceous post-collisional granitoids at Shapinggou, Dabie Orogen: Implications for crustal architecture and porphyry Mo mineralization. *Lithos* 184, 393-415.
- Wang, H.Z., Chen, R., Sun, L.Q., Ling, H.F., Zhao, Y.D., Lan, H.F. (2015a) Magma mixing and crust–mantle interaction in Southeast China during the Early Cretaceous. Evidence from the Furongshan granite porphyry and mafic microgranular enclaves. *Journal of Asian Earth Sciences* 111, 72-87.
- Wang, J.X., Nie, F.J., Zhang, X.N., Jiang, S.H. (2016) Molybdenite Re–Os, zircon U–Pb dating and Lu–Hf isotopic analysis of the Xiaerchulu Au deposit, Inner Mongolia Province, China. *Lithos* 261, 356-372.
- Wang, K.X., Chen, W.F., Chen, P.R., Ling, H.F., Huang, H. (2015b) Petrogenesis and geodynamic implications of the Xiema and Ziyunshan plutons in Hunan Province, South China. *Journal of Asian Earth Sciences* 111, 919-935.
- Wang, K.X., Sun, T., Chen, R., Ling, H.F., Xiang, T. F. (2013a) The geochronological and geochemical constraints on the petrogenesis of the Early Mesozoic A-type granite and diabase in northwestern Fujian province. *Lithos* 179, 364-381.
- Wang, L., Guo, J., Peng, P., Liu, F., Windley, B. F. (2015c) Lithological units at the boundary zone between the Jining and Huai'an Complexes (central-northern margin of the North China Craton): A Paleoproterozoic tectonic mélange? *Lithos* 227, 205-224.
- Wang, Q., Wyman, D.A., Li, Z.X., Bao, Z.W., Zhao, Z.H., Wang, Y.X., Jian, P., Yang, Y.H., Chen, L.L. (2010) Petrology, geochronology and geochemistry of ca. 780 Ma A-type granites in South China. Petrogenesis and implications for crustal growth during the breakup of the supercontinent Rodinia. *Precambrian Research* 178, 185-208.
- Wang, R., Richards, J., Hou, Z.Q., An, F., Creaser, R.A. (2015d) Zircon U–Pb age and Sr–Nd–Hf–O isotope geochemistry of the Paleocene–Eocene igneous rocks in western Gangdese. Evidence for the timing of Neo-Tethyan slab breakoff. *Lithos* 224–225, 179-194.
- Wang, X.S., Hu, R.Z., Bi, X.W., Leng, C.B., Pan, L.C., Zhu, J.J., Chen, Y.W. (2014b) Petrogenesis of Late Cretaceous I-type granites in the southern Yidun Terrane: new constraints on the Late Mesozoic tectonic evolution of the eastern Tibetan Plateau. *Lithos* 208, 202-219.
- Wang, Y., Xing, X., Cawood, P. A., Lai, S., Xia, X., Fan, W., Zhang, F. (2013b) Petrogenesis of early Paleozoic peraluminous granite in the Sibumasu Block of SW Yunnan and diachronous accretionary orogenesis along the northern margin of Gondwana. *Lithos* 182, 67-85.
- Weis, D., Kieffer, B., Hanano, D., Nobre-Silva, I., Barling, J., Pretorius, W., Maerschalk, C., Mattielli, N. (2007) Hf isotope compositions of U.S. Geological survey reference materials. *Geochemistry, Geophysics, Geosystems* 8, Q06006.
- Wiedenbeck, M., Hanchar, J.M., Peck, W.H., Sylvester, P., Valley, J., Whitehouse, M., Kronz, A., Morishita, Y., Nasdala, L., Fiebig, J., Franchi, I., Girard, J.P., Greenwood, R.C., Hinton, R., Kita, N., Mason, P.R.D., Norman, M., Ogasawara, M., Piccoli, R., Rhede, D., Satoh, H., Schulz-Dobrick, B., Skar, O., Spicuzza, M.J., Terada, K., Tindle, A., Togashi, S., Vennemann, T., Xie, Q., Zheng, Y.F. (2004) Further characterisation of the 91500 zircon crystal. *Geostandards and Geoanalytical Research* 28, 9-39.
- Wu, R.X., Zheng, Y.F., Wu, Y.B., Zhao, Z.F., Zhang, S.B., Liu, X., Wu, F.Y. (2006) Reworking of juvenile crust: element and isotope evidence from Neoproterozoic granodiorite in South China. *Precambrian Research* 146, 179-212.
- Wu, T., Xiao, L., Wilde, S.A., Ma, C.Q., Zhou, J.X. (2017) A mixed source for the Late Triassic Garzê–Daocheng granitic belt and its implications for the tectonic evolution of the Yidun arc belt, eastern Tibetan Plateau. *Lithos* 288, 214-230.
- Xia, R., Deng, J., Qing, M., Li, W., Guo, X., & Zeng, G. (2017) Petrogenesis of ca. 240 Ma intermediate and felsic intrusions in the Nan'getan: Implications for crust–mantle interaction and geodynamic process of the East Kunlun Orogen. *Ore Geology Reviews* 90, 1099-1117.
- Xia, Y., Xu, X., Liu, L. (2016) Transition from adakitic to bimodal magmatism induced by the paleo-Pacific plate subduction and slab rollback beneath SE China. Evidence from petrogenesis and tectonic setting of the dike swarms. *Lithos* 244, 182-204.
- Xia, Y., Xu, X., Zou, H., Liu, L. (2014) Early Paleozoic crust–mantle interaction and lithosphere delamination in South China Block: evidence from geochronology, geochemistry, and Sr–Nd–Hf isotopes of granites. *Lithos* 184, 416-435.
- Xia, Y., Xu, X.S., Zhu, K.Y. (2012) Paleoproterozoic S- and A-type granites in southwestern Zhejiang. Magmatism, metamorphism and implications for the crustal evolution of the Cathaysia basement. *Precambrian Research* 216–219, 177-207.
- Xiao, B., Li, Q., He, S., Chen, X., Liu, S., Wang, Z., Chen, J. (2017) Contrasting geochemical signatures between Upper Triassic Mo-hosting and barren granitoids in the central segment of the South Qinling orogenic belt, central China: Implications for Mo exploration. *Ore Geology Reviews* 81, 518-534.
- Xin, W., Sun, F.Y., Li, L., Yan, J.M., Zhang, Y.T., Wang, Y.C., Shen, T.S., Yang, Y.J. (2018) The Wulonggou metaluminous A2-type granites in the Eastern Kunlun Orogenic Belt, NW China. Rejuvenation of subduction-related felsic crust and implications for post-collision extension. *Lithos* 312–313, 108-127.
- Xu, B., Jiang, S.Y., Wang, R., Ma, L., Zhao, K.D., Yan, X. (2015) Late Cretaceous granites from the giant Dulong Sn-polymetallic ore district in Yunnan Province, South China: Geochronology, geochemistry, mineral chemistry and Nd–Hf isotopic compositions. *Lithos* 218, 54-72.
- Yan, Q.H., Li, S.S., Qiu, Z.W., Wang, H., Wei, X.P., Dong, R., Zhang, X.Y. (2017) Geochronology, geochemistry and Sr–Nd–Hf–S–Pb isotopes of the Early Cretaceous Taoxihu Sn deposit and related granitoids, SE China. *Ore Geology Reviews* 89, 350-368.
- Yan, Q.H., Wang, H., Qiu, Z.W., Wei, X., Dong, R., Zhou, K. (2018) Origin of Early Cretaceous A-type granite and related Sn mineralization in the Sanjiaowo deposit, eastern Guangdong, SE China and its tectonic implication. *Ore Geology Reviews* 93, 60-80.
- Yang, J.H., Peng, J.T., Zheng, Y.F., Hu, R.Z., Bi, X.W., Zhao, J.H., Zhang, B.L. (2016a) Petrogenesis of the Mesozoic Shuikoushan peraluminous I-type granodioritic intrusion in Hunan Province, South China. Middle–lower crustal reworking in an extensional tectonic setting. *Journal of Asian Earth Sciences* 123, 224-242.
- Yang, J.H., Wu, F.Y., Chung, S.L., Simon, A.W., Chu, M.F. (2006) A hybrid origin for the Qianshan A-type granite, northeast China: Geochemical and Sr–Nd–Hf isotopic evidence. *Lithos* 89, 89-106.
- Yang, L.Q., Deng, J., Dilek, Y., Meng, J.Y., Gao, X., Santosh, M., Yan, H. (2016b) Melt source and evolution of I-type granitoids in the SE Tibetan Plateau: Late Cretaceous magmatism and mineralization driven by collision-induced transtensional tectonics. *Lithos* 245, 258-273.
- Yang, S.Y., Jiang, S.Y., Zhao, K.D., Jiang, Y.H., Ling, H.F., Luo, L. (2012) Geochronology, geochemistry and tectonic significance of two Early Cretaceous A-type granites in the Gan-Hang Belt, Southeast China. *Lithos* 150, 155-170.
- Yang, Y.L., Ni, Yan, J., Wu, C.Z., Dai, B.Z., Xu, Y.F. (2017) Early to late Yanshanian I-type granites in Fujian Province, SE China. Implications for the tectonic setting and Mo mineralization. *Journal of Asian Earth Sciences* 137, 194-219.
- Ye, X.T., Zhang, C.L., Santosh, M., Zhang, J., Fan, X.K., Zhang, J.J. (2016) Growth and evolution of Precambrian continental crust in the southwestern Tarim terrane. New evidence from the ca. 1.4Ga A-type granites and Paleoproterozoic intrusive complex. *Precambrian Research* 275, 18-34.
- Yin, J., Chen, W., Xiao, W., Yuan, C., Windley, B.F., Yu, S., Cai, K. (2017) Late Silurian–early Devonian adakitic granodiorite, A-type and I-type granites in NW Junggar,



- NW China. Partial melting of mafic lower crust and implications for slab roll-back. *Gondwana Research* 43, 55-73.
- Yu, Y., Huang, X.L., He, L., Li, J. (2016) I-type granitoids associated with the early Paleozoic intracontinental orogenic collapse along pre-existing block boundary in South China. *Lithos* 248–251, 353–365.
- Yu, Y., Sun, M., Long, X., Li, P., Zhao, G., Kröner, A., Yang, J. (2017) Whole-rock Nd–Hf isotopic study of I-type and peraluminous granitic rocks from the Chinese Altai. Constraints on the nature of the lower crust and tectonic setting. *Gondwana Research* 47, 131–141.
- Yuan, L., Zhang, X., Xue, F., Liu, F. (2016) Juvenile crustal recycling in an accretionary orogen. Insights from contrasting Early Permian granites from central Inner Mongolia, North China. *Lithos* 264, 524–539.
- Zhang, C., Liu, D., Luo, Q., Liu, L., Zhang, Y., Zhu, D., Dai, Q. (2018a) An evolving tectonic environment of Late Carboniferous to Early Permian granitic plutons in the Chinese Altai and Eastern Junggar terranes, Central Asian Orogenic Belt, NW China. *Journal of Asian Earth Sciences* 159, 185–208.
- Zhang, C., Liu, L., Santosh, M., Luo, Q., Zhang, X. (2017a) Sediment recycling and crustal growth in the Central Asian Orogenic Belt: evidence from Sr–Nd–Hf isotopes and trace elements in granitoids of the Chinese Altay. *Gondwana Research* 47, 142–160.
- Zhang, C., Santosh, M., Liu, L., Luo, Q., Zhang, X., Liu, D. (2018b) Early Silurian to Early Carboniferous ridge subduction in NW Junggar. Evidence from geochronological, geochemical, and Sr–Nd–Hf isotopic data on alkali granites and adakites. *Lithos* 300–301, 314–329.
- Zhang, C., Santosh, M., Luo, Q., Jiang, S., Liu, L.F., Liu, D. (2019) Impact of residual zircon on Nd–Hf isotope decoupling during sediment recycling in subduction zone. *Geoscience Frontiers* 10, 241–251.
- Zhang, C.L., Zou, H.B. (2013) Permian A-type granites in Tarim and western part of Central Asian Orogenic Belt (CAOB): Genetically related to a common Permian mantle plume? *Lithos* 172–173, 47–60.
- Zhang, D.H., Wei, J.H., Fu, L.B., Schmitt, A.K., Wang, D.Z., Tan, J., Liu, J.K. (2017b) Petrogenesis and thermal overprint of S-type granites in Helanshan region, North China Craton: Constraints on the 1.90 Ga khondalites decompression melting and 1.32 Ga tectono-thermal event. *Precambrian Research* 303, 660–672.
- Zhang, L., Chen, Z., Li, S., Santosh, M., Huang, G., Tian, Z. (2017c) Isotope geochronology, geochemistry, and mineral chemistry of the U-bearing and barren granites from the Zhuguangshan complex, South China: Implications for petrogenesis and uranium mineralization. *Ore Geology Reviews* 91, 1040–1065.
- Zhang, L., Zhang, R., Hu, Y., Liang, J., Ouyang, Z., He, J., Chen, Y.X., Guo, J., Sun, W. (2017d) The formation of the Late Cretaceous Xishan Sn–W deposit, South China. Geochronological and geochemical perspectives. *Lithos* 290–291, 253–268.
- Zhang, S.B., Zheng, Y.F., Zhao, Z.F., Wu, Y.B., Yuan, H., Wu, F.Y. (2008) Neoproterozoic anatexis of Archean lithosphere: geochemical evidence from felsic to mafic intrusions at Xiaofeng in the Yangtze Gorge, South China. *Precambrian Research* 163, 210–238.
- Zhang, W., Chen, H., Han, J., Zhao, L., Huang, J., Yang, J., Yan, X. (2016) Geochronology and geochemistry of igneous rocks in the Bailingshan area: Implications for the tectonic setting of late Paleozoic magmatism and iron skarn mineralization in the eastern Tianshan, NW China. *Gondwana Research* 38, 40–59.
- Zhang, X., Zhang, H. (2014) Geochronological, geochemical, and Sr–Nd–Hf isotopic studies of the Baiyanghe A-type granite porphyry in the Western Junggar. Implications for its petrogenesis and tectonic setting. *Gondwana Research* 25, 1554–1569.
- Zhang, Y., Yang, J.H., Chen, J.Y., Wang, H., Xiang, Y.X. (2017e) Petrogenesis of Jurassic tungsten-bearing granites in the Nanling Range, South China. Evidence from whole-rock geochemistry and zircon U–Pb and Hf–O isotopes. *Lithos* 278–281, 166–180.
- Zhang, Y., Yang, J.H., Sun, J. F., Zhang, J.H., Chen, J.Y., Li, X.H. (2015) Petrogenesis of Jurassic fractionated I-type granites in Southeast China. Constraints from whole-rock geochemical and zircon U–Pb and Hf–O isotopes. *Journal of Asian Earth Sciences* 111, 268–283.
- Zhao, H.X., Jiang, S.Y., Frimmel, H.E., Dai, B.Z., Ma, L. (2012) Geochemistry, geochronology and Sr–Nd–Hf isotopes of two Mesozoic granitoids in the Xiaoqinling gold district. Implication for large-scale lithospheric thinning in the North China Craton. *Chemical Geology* 294–295, 173–189.
- Zhao, J.H., Pandit, M.K., Wang, W., Xia, X. (2018) Neoproterozoic tectonothermal evolution of NW India. Evidence from geochemistry and geochronology of granitoids. *Lithos* 316–317, 330–346.
- Zhao, J.L., Qiu, J.S., Liu, L., Wang, R.Q. (2015a) Geochronological, geochemical and Nd–Hf isotopic constraints on the petrogenesis of Late Cretaceous A-type granites from the southeastern coast of Fujian Province, South China. *Journal of Asian Earth Sciences* 105, 338–359.
- Zhao, J.L., Qiu, J.S., Liu, L., Wang, R.Q. (2016a) The Late Cretaceous I- and A-type granite association of southeast China. Implications for the origin and evolution of post-collisional extensional magmatism. *Lithos* 240–243, 16–33.
- Zhao, K.D., Jiang, S.Y., Chen, W.F., Chen, R., Ling, H.F. (2013) Zircon U–Pb chronology and elemental and Sr–Nd–Hf isotope geochemistry of two Triassic A-type granites in South China. Implication for petrogenesis and Indosinian transtensional tectonism. *Lithos* 160–161, 292–306.
- Zhao, K.D., Jiang, S.Y., Ling, H.F., Sun, T., Chen, W.F., Chen, P.R., Pu, W. (2016b) Late Triassic U-bearing and barren granites in the Miao’ershan batholith, South China: Petrogenetic discrimination and exploration significance. *Ore Geology Reviews* 77, 260–278.
- Zhao, P., Xu, B., Jahn, B.M. (2017a) The Mongol-Okhotsk Ocean subduction-related Permian peraluminous granites in northeastern Mongolia: Constraints from zircon U–Pb ages, whole-rock elemental and Sr–Nd–Hf isotopic compositions. *Journal of Asian Earth Sciences* 144, 225–242.
- Zhao, T., Zhou, M.F. (2009) Geochemical constraints on the tectonic setting of Paleoproterozoic A-type granites in the southern margin of the North China Craton. *Journal of Asian Earth Sciences* 36, 183–195.
- Zhao, X.F., Zhou, M.F., Li, J.W., Wu, F.Y. (2008) Association of Neoproterozoic A- and I-type granites in South China. Implications for generation of A-type granites in a subduction-related environment. *Chemical Geology* 257, 1–15.
- Zhao, Z., Wei, J., Fu, L., Liang, S., Zhao, S. (2017b) The Early Paleozoic Xitieshan syn-collisional granite in the North Qaidam ultrahigh-pressure metamorphic belt, NW China: Petrogenesis and implications for continental crust growth. *Lithos* 278, 140–152.
- Zhao, Z.F., Gao, P., Zheng, Y.F. (2015b) The source of Mesozoic granitoids in South China: Integrated geochemical constraints from the Taoshan batholith in the Nanling Range. *Chemical Geology* 395, 11–26.
- Zheng, W., Mao, J.W., Zhao, H.J., Ouyang, H.G., Zhao, C.S., Yu, X.F. (2017a) Geochemistry, Sr–Nd–Pb–Hf isotopes systematics and geochronological constraints on petrogenesis of the Xishan A-type granite and associated W–Sn mineralization in Guangdong Province, South China. *Ore Geology Reviews* 88, 739–752.
- Zheng, W., Mao, J.W., Zhao, H.J., Zhao, C.S., Yu, X.F. (2017b) Two Late Cretaceous A-type granites related to the Yingwuling W–Sn polymetallic mineralization in Guangdong province, South China: Implications for petrogenesis, geodynamic setting, and mineralization. *Lithos* 274–275, 106–122.
- Zheng, Y.F., Wu, R.X., Wu, Y.B., Zhang, S.B., Yuan, H., Wu, F.Y. (2008) Rift melting of juvenile arc-derived crust: geochemical evidence from Neoproterozoic volcanic and granitic rocks in the Jiangnan Orogen, South China. *Precambrian Research* 163, 351–383.
- Zheng, Z., Chen, Y.J., Deng, X.H., Yue, S.W., Chen, H.J., Wang, Q.F. (2018) Origin of the Bashierxi monzogranite, Qiman Tagh, East Kunlun Orogen, NW China: A magmatic response to the evolution of the Proto-Tethys Ocean. *Lithos* 296, 181–194.
- Zhong, H., Campbell, I. H., Zhu, W. G., Allen, C. M., Hu, R. Z., Xie, L. W., He, D. F. (2011) Timing and source constraints on the relationship between mafic and felsic intrusions in the Emeishan large igneous province. *Geochimica et Cosmochimica Acta* 75, 1374–1395.



- Zhong, L., Wang, B., Alexeiev, D., Cao, Y., Biske, Y.S., Liu, H., Zhai, Y.A., Xing, L. (2017) Paleozoic multi-stage accretionary evolution of the SW Chinese Tianshan. New constraints from plutonic complex in the Nalati Range. *Gondwana Research* 45, 254-274.
- Zhong, Y., Ma, C., Zhang, C., Wang, S., She, Z., Liu, L., Xu, H. (2013) Zircon U-Pb age, Hf isotopic compositions and geochemistry of the Silurian Fengdingshan I-type granite Pluton and Taoyuan mafic-felsic Complex at the southeastern margin of the Yangtze Block. *Journal of Asian Earth Sciences* 74, 11-24.
- Zhou, G., Wu, Y., Gao, S., Yang, J., Zheng, J., Qin, Z., Wang, H., Yang, S. (2015a) The 2.65 Ga A-type granite in the northeastern Yangtze craton. Petrogenesis and geological implications. *Precambrian Research* 258, 247-259.
- Zhou, G., Wu, Y., Wang, H., Qin, Z., Zhang, W., Zheng, J., Yang, S. (2017) Petrogenesis of the Huashanguan A-type granite complex and its implications for the early evolution of the Yangtze Block. *Precambrian Research* 292, 57-74.
- Zhou, Y.Y., Zhao, T.P., Wang, C.Y., Hu, G.H. (2011) Geochronology and geochemistry of 2.5 to 2.4Ga granitic plutons from the southern margin of the North China Craton. Implications for a tectonic transition from arc to post-collisional setting. *Gondwana Research* 20, 171-183.
- Zhou, Z.M., Ma, C.Q., Wang, L.X., Chen, S.G., Xie, C.F., Li, Y., Liu, W. (2018) A source-depleted Early Jurassic granitic pluton from South China. Implication to the Mesozoic juvenile accretion of the South China crust. *Lithos* 300-301, 278-290.
- Zhou, Z.H., Mao, J.W., Lyckberg, R. (2012) Geochronology and isotopic geochemistry of the A-type granites from the Huanggang Sn-Fe deposit, southern Great Hinggan Range, NE China. Implication for their origin and tectonic setting. *Journal of Asian Earth Sciences* 49, 272-286.
- Zhou, Z.H., Mao, J.W., Wu, X.L., Ouyang, H.G. (2015b) Geochronology and geochemistry constraints of the Early Cretaceous Taibudai porphyry Cu deposit, northeast China, and its tectonic significance. *Journal of Asian Earth Sciences* 103, 212-228.
- Zhu, D.C., Mo, X.X., Niu, Y., Zhao, Z.D., Wang, L.Q., Pan, G.T., Wu, F.Y. (2009) Zircon U-Pb dating and in-situ Hf isotopic analysis of Permian peraluminous granite in the Lhasa terrane, southern Tibet: implications for Permian collisional orogeny and paleogeography. *Tectonophysics* 469, 48-60.
- Zhu, J.J., Hu, R.Z., Bi, X.W., Zhong, H., Chen, H. (2011) Zircon U-Pb ages, Hf-O isotopes and whole-rock Sr-Nd-Pb isotopic geochemistry of granitoids in the Jinshajiang suture zone, SW China. Constraints on petrogenesis and tectonic evolution of the Paleo-Tethys Ocean. *Lithos* 126, 248-264.
- Zhu, Y., Zhang, D., Wang, L., Dai, Y., Xi, A. (2016) SHRIMP zircon UPb dating, geochemistry and SrNdHf isotopes of the Tongcun ore-bearing porphyry in NW Zhejiang Province, South China. *Journal of Geochemical Exploration* 172, 50-61.
- Zi, J.W., Cawood, P.A., Fan, W.M., Tohver, E., Wang, Y.J., McCuaig, T.C. (2012) Generation of Early Indosian enriched mantle-derived granitoid pluton in the Sanjiang Orogen (SW China) in response to closure of the Paleo-Tethys. *Lithos* 140, 166-182.

